

A reconstruction of extratropical Indo-Pacific sea-level pressure patterns during the Medieval Climate Anomaly

Ian D. Goodwin · Stuart Browning · Andrew M. Lorrey · Paul A. Mayewski · Steven J. Phipps · Nancy A. N. Bertler · Ross P. Edwards · Tim J. Cohen · Tas van Ommen · Mark Curran · Cameron Barr · J. Curt Stager

Received: 28 May 2013 / Accepted: 29 July 2013 / Published online: 28 August 2013
© Springer-Verlag Berlin Heidelberg 2013

Abstract Subtropical and extratropical proxy records of wind field, sea level pressure (SLP), temperature and hydrological anomalies from South Africa, Australia/New Zealand, Patagonian South America and Antarctica were used to reconstruct the Indo-Pacific extratropical southern hemisphere sea-level pressure anomaly (SLPa) fields for the Medieval Climate Anomaly (MCA ~700–1350 CE) and transition to the Little Ice Age (LIA 1350–1450 CE). The multivariate array of proxy data were simultaneously evaluated against global climate model output in order to identify climate state analogues that are most consistent with the majority of proxy data. The mean SLP and SLP anomaly patterns derived from these analogues illustrate

the evolution of low frequency changes in the extratropics. The Indo-Pacific extratropical mean climate state was dominated by a strong tropical interaction with Antarctica emanating from: (1) the eastern Indian and south-west Pacific regions prior to 1100 CE, then, (2) the eastern Pacific evolving to the central Pacific La Niña-like pattern interacting with a +ve SAM to 1300 CE. A relatively abrupt shift to –ve SAM and the central Pacific El Niño-like pattern occurred at ~1300. A poleward (equatorward) shift in the subtropical ridge occurred during the MCA (MCA–LIA transition). The Hadley Cell expansion in the Australian and Southwest Pacific, region together with the poleward shift of the zonal westerlies is contemporaneous

I. D. Goodwin (✉) · S. Browning
Marine Climate Risk Group and Environmental Science,
Macquarie University, Sydney, NSW 2109, Australia
e-mail: Ian.Goodwin@mq.edu.au

A. M. Lorrey
National Climate Centre, National Institute of Water
and Atmospheric Research, Auckland, New Zealand

P. A. Mayewski
Climate Change Institute, University of Maine,
Orono, ME 04469-5790, USA

S. J. Phipps
Climate Change Research Centre, ARC Centre of Excellence
for Climate System Science, University of New South Wales,
Sydney, NSW 2052, Australia

N. A. N. Bertler
Joint Antarctic Research Institute, Victoria University and GNS
Science, PO Box 600, Wellington 6012, New Zealand

R. P. Edwards
Desert Research Institute, Nevada System of Higher Education,
Reno, NV 89512, USA

R. P. Edwards
Department of Imaging and Applied Physics, Curtin University,
Perth, WA 6845, Australia

T. J. Cohen
GeoQuEST Research Centre, School of Earth
and Environmental Sciences, University of Wollongong,
Wollongong, NSW 2522, Australia

T. van Ommen · M. Curran
Australian Antarctic Division, Kingston, TAS 7050, Australia

T. van Ommen · M. Curran
Antarctic Climate and Ecosystems CRC,
University of Tasmania, Hobart, TAS, Australia

C. Barr
Discipline of Geography, Environment and Population,
University of Adelaide, North Terrace,
Adelaide, SA 5005, Australia

J. C. Stager
Natural Sciences, Paul Smith's College,
Paul Smiths, NY 12970, USA

with previously reported Hadley Cell expansion in the North Pacific and Atlantic regions, and suggests that bipolar climate symmetry was a feature of the MCA.

Keywords Medieval Climate Anomaly · Extratropical · Southern Annular Mode · Pacific South American Mode · Paleo-sea-level pressure reconstruction

1 Introduction

Proxy climate indicators for the Northern Hemisphere and particularly, the North Atlantic region have defined a period of widespread warm climate anomalies (Bradley et al. 2003; Lamb 1965; Mann et al. 2009; Jones et al. 2009; Diaz et al. 2011; PAGES 2k Network 2013) and ‘persistent drought’ anomalies across the North and Central Americas during Medieval times, that is commonly known as the Medieval Climate Anomaly (MCA) (Stine 1994). The MCA has been associated with an extreme multi-centennial shift to positive North Atlantic Oscillation (NAO) (Trouet et al. 2009) and an extreme positive Atlantic Multidecadal Oscillation (AMO) (Knudsen et al. 2011). Coupled to the Atlantic anomalies is a shift in the tropical Pacific mean climate state during the MCA. The pattern during this time resembles a La Niña-like state akin to the La Niña-like phase of the Pacific Decadal Oscillation (PDO) (MacDonald and Case 2005; Rein et al. 2004, 2005) or Interdecadal Pacific Oscillation (IPO) as it is known in the Southwest Pacific (Folland et al. 2002). Recently, Oglesby et al. (2011) found that the North American and North Pacific climate anomalies were the product of the combined shifts in the AMO and PDO mean state. There is also increasing evidence for a northward shift of the Inter-Tropical Convergence Zone into the NH during the MCA (Sachs et al. 2009; Sachs and Myhrvold 2011).

In contrast, the Southern Hemisphere (SH) paleo-temperature, hydrological and atmospheric circulation evidence has been scant to date and evidence is often conflicting between regions. This is possibly the result of too few available proxy data, or perhaps indicates a more heterogeneous climate change across the SH, as exemplified by the recent regional surface temperature reconstructions for the past 1,000 years (PAGES 2k Network 2013). Many SH climate anomalies have often been described in terms of the shift in ENSO mean state towards more La Niña-like conditions during the MCA (Khider et al. 2011). One example is Palmyra Island, nested in the central tropical Pacific Niño 3.4 region, where the coolest proxy sea-surface temperature anomalies (SSTa) in the past 1,100 years occurred from ~900 to 1000 CE. In addition, that site indicates cooler than modern SSTa’s occurred

during ~1150–1220 CE, with a shift towards the El Niño mean state as indicated by a warm SSTa from ~1240 to 1300 CE (Cobb et al. 2003, 2011). In the eastern Tropical Pacific (Galapagos Islands, Niño 1+2 region), more dry (wet) conditions consistent with more La Niña-like (more El Niño-like) climate occurred during the period 800–1000 CE (1000–1300 CE) (Conroy et al. 2008). The cool eastern Pacific SSTa are synchronous with the persistent drought conditions from the mid-latitude western North America, Central America into sub-tropical South America (Rein et al. 2004; MacDonald and Case 2005).

In the western Pacific, the western edge of the Indo-Pacific Warm Pool (IPWP) in the southern Makassar Strait and Java Sea near the equator (0–10°S) at 110–120°E was as warm as modern times from 1000 to 1250 CE, with significantly cooler SST’s from 400 to 950 CE and post 1300 CE (Newton et al. 2006; Linsley et al. 2008, 2010; Oppo et al. 2009). The period of cooler western Pacific SST is associated with southward displacement of the East Asian summer monsoon (EASM), and are potentially linked to persistent drought episodes in Indonesia (after Rodysill et al. 2011 Griffiths et al. 2011). Tierney et al. (2010a) have demonstrated that the IPWP hydrological changes during the MCA were associated with a strong EASM, a weak Indonesian monsoon, and changes in the Walker Circulation. In the sub-tropical southwest Pacific, cool SSTa and low relative sea-level at the eastern-most edge of the IPWP in the sub tropical Central Pacific (Southern Cook Islands) were reported in the 900 to 1000 CE period (Goodwin and Harvey 2008). Coupled to these shifts is the interpreted southwestwards migration of the South Pacific Convergence Zone (SPCZ) (Linsley et al. 2008).

Graham et al. (2010) modelled atmospheric circulation during the MCA with assumptions based on the previous finding by Mann et al. (2009) that the shift in climate between the MCA and subsequent Little Ice Age (LIA) was associated with reversals in the tropical Indo-Pacific SST gradient and the ocean thermostat response (Clement et al. 1996). It was assumed that a larger-than-present east–west SST gradient occurred during the MCA (Clement et al. 1996; Mann et al. 2009) coupled with a strengthened Walker Circulation associated with the shift towards a La Niña-like mean state. Graham et al. (2010) found good agreement between proxy data and model output in the NH, but it was inconclusive in the SH extratropics. However, little is known about the corresponding SH extratropical circulation and interaction with ENSO modes during the MCA, and whether bipolar symmetry or asymmetry in climate anomalies occurred. For example, Mohtadi et al. (2007) concluded that an equatorward shift in the westerlies had occurred at 44°S on the Chilean coast during the MCA (with a northward peak during 1250–1350 CE),

transporting an enhanced cold current. In the high Southern latitudes the Siple Dome (SD) sea-salt record indicates an extreme weakening of the Amundsen Sea Low in the early MCA (700–1000 CE) (Kreutz et al. 2000; Mayewski et al. 2005).

Both these examples indicate an atmospheric circulation bias towards a negative phase of the Southern Annular Mode (SAM) (Thompson and Wallace 2000). Over the past 50 years, the SAM has been the leading EOF, accounting for an equivalent 22 % of atmospheric pressure-field variability. The SAM describes variations in the zonality of circumpolar atmospheric circulation and is based on the oscillation of atmospheric mass between polar and mid-latitudes (Thompson and Wallace 2000). While the SAM dominates pressure changes in the vicinity of the Antarctic continent and influences the intensity and latitude of circumpolar westerlies, the Pacific South American (PSA) Modes contribute mostly to pressure changes throughout the troposphere in the South Pacific to South Atlantic sectors between 50°S and 60°S. The PSA modes correspond to the 2nd and 3rd EOF's of the SH pressure field accounting for 22 % of the pressure-field variability (Mo and Higgins 1998; Hall and Visbeck 2002; Visbeck and Hall 2004). We use the definitions for PSA1 and PSA2 from Mo and Paegle (2001).

In this paper we reconstruct the SLPa patterns over the extratropical Indo-Pacific region for the SH MCA. We use multivariate paleoclimate proxies from the subtropics to the extratropics and develop synoptic climate analogues

from a coupled atmosphere–ocean global climate model (AOGCM) simulation spanning 10,000 years of natural variability. We first present a synthesis of proxy climate data covering the SH MCA. We then investigate the spatial and temporal proxy evidence for atmospheric pressure, wind field, hydrological and surface temperature change in Africa, Australia, New Zealand, Antarctica and Patagonian South America. We also investigate the relationship between the evolution of the SLPa patterns and describe the changes in the SLP field during the MCA with respect to the combination and hierarchy of the three EOF loading patterns in the control simulation of the modern climate (Fig. 1), and interpret mean state changes with respect to the time-varying AMO or PDO/ENSO-related ‘atmospheric bridge’ teleconnections (after Liu and Alexander 2007).

2 Multi-proxy indicators of atmospheric circulation shifts in the southern hemisphere

In previous studies, we have documented our research in obtaining paleoclimate proxy data from field studies at 12 regions across the SH. Each of these regions is intrinsically linked to atmospheric circulation variability and planetary wave behaviour in the sub-tropical to extratropical SH during the MCA. The geographic location and types of proxy data are listed in Table 1, together with key paleoclimate proxy data, previously published by other researchers.

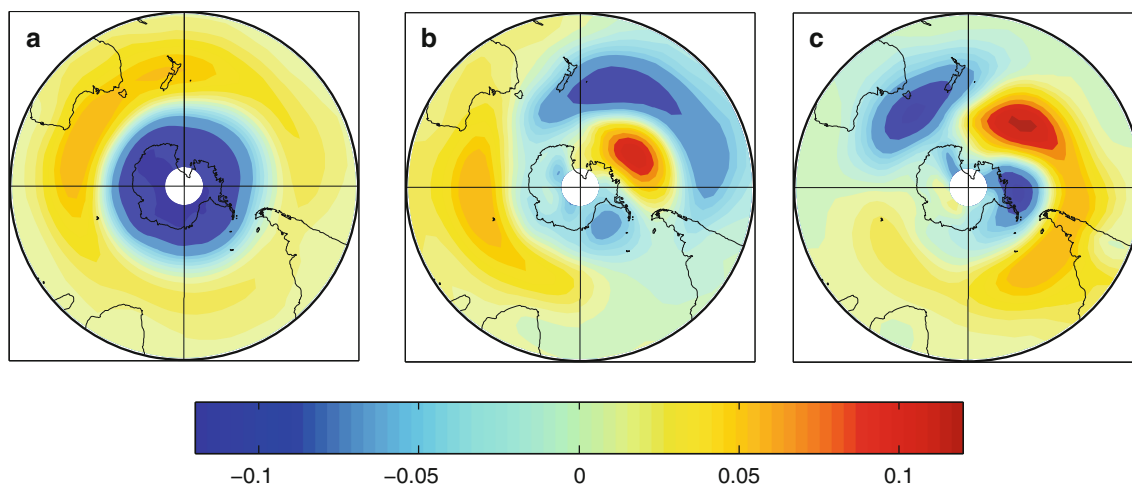


Fig. 1 The empirical orthogonal function (EOF) loading patterns for the first 3 EOF's of the 10,000 year AOGCM (Mk3L) control simulation, May to November southern hemisphere sea-level pressure (SLP) field between 20°S and 82°S are shown. To ensure equal area representation each gridpoint was multiplied by the cosine of the latitude prior to decomposition. The cosine factor was multiplied back in prior to plotting the loading patterns. These EOF loading patterns correspond to the leading extratropical climate modes; (a) Mode 1—Southern Annular Mode (SAM); (b) Mode 2—Pacific South

American (PSA1); and (c) Mode 3—Pacific South American (PSA2); according to the definitions of Visbeck and Hall (2004), Mo and Higgins (1998), Renwick and Revell (1999), and Karoly (1989). Note that these patterns are shown for: (a) the +ve phase of the SAM; (b) PSA1+ve; and (c) PSA2–ve. The sign of the loading patterns are reversed for the opposite phase of each mode. Each EOF accounts for the following variance; EOF1 (39 %), EOF2 (12 %), and EOF3 (7.2 %)

Table 1 List of proxy climate data that were used to develop regional proxy sea-level pressure analogues in the SLP reconstructions for the MCA

No.	Location	Proxy data type	Variable	Lat °S	Long °E	Region	References
1	Chile-Laguna Aculeo	Sediment core	Temperature	-33.75	288.25	South America	von Gunten et al. (2009)
2	Cook Islands	Coral	SSTA	-21.5	200.5	S.W. Pacific Ocean	Goodwin and Harvey (2008)
3	Lake Callabonna	Paleoshoreline	Precipitation	-30	139	Australia	Cohen et al. (2012)
4	Lake Frome	Paleoshoreline	Precipitation	-30	139	Australia	Cohen et al. (2011)
5	Lake Surprise, Victoria	Lake Sediment Core	Precipitation	-38	141	Australia	Barr (2010)
6	Lake Verlorenvlei	Lake sediments	Precipitation	-33	18.3	South Africa	Stager et al. (2012)
7	Law Dome DSS	Ice Core d18o	SLP	-66	112	E. Antarctica	Moy (pers. comm. 2011)
8	Law Dome DSS	Ice core Na	SLP	-66	112	E. Antarctica	Goodwin et al. (2004)
9	Makapansgat Valley	Speleothems	Precipitation	-24	28	South Africa	Holmgren et al. (1999); Tyson (2000); Cook et al. (2000)
10	Mt Read Tasmania	Tree rings	Temperature	-42	145	Australia	Cook et al. (2000)
11	Northern NSW Coast, SE Queensland coast	Dune sediments relic coastlines	Wave climate	-25.80 to -32.0	153.00	Australia	Goodwin et al. (2006) Goodwin et al. (in Prep)
12	NZ regional precipitation	Multiproxy	Precipitation	-37 to -45	168 to 77	New Zealand	Lorrey et al. (2008)
13	NZ-Southern Glaciers	Glacial sediments	Precipitation	-43	170	New Zealand	Schaefer et al. (2009)
14	Oroko Swamp	Tree rings	Temperature	-43	170	New Zealand	Cook et al. (2002)
15	Patagonia Lago Guanaco	Sediment core	Precipitation	-52	287	South America	Moy et al. (2008)
16	Patagonia-Tree Rings	Tree rings	Precipitation	-41	289	South America	Villalba (1990)
17	Siple Dome SD	Ice Core Na	SLP	-81	212	W. Antarctica	Kreutz et al. (2000)
18	South America Temperature	Multiproxy	Temperature	-25 to -50	287 to 290	South America	Neukom et al. (2010)
19	South Georgia Is.	Glacial Lake sediments	Temperature	-54	324	South Atlantic	Rosqvist and Schuber (2003)
20	South Orkney Is.	Lake sediment d18o	Temperature	-60.5	314.5	South Atlantic	Noon et al. (2003)
21	Victoria Lower Glacier	Ice core deuterium excess	Temperature	-77.2	166.5	E. Antarctica	Bertler et al. (2011)
22	Victoria Lower Glacier	Ice core Fe	SLP	-77.2	166.5	E. Antarctica	Bertler et al. (2011)

2.1 East and West Antarctica

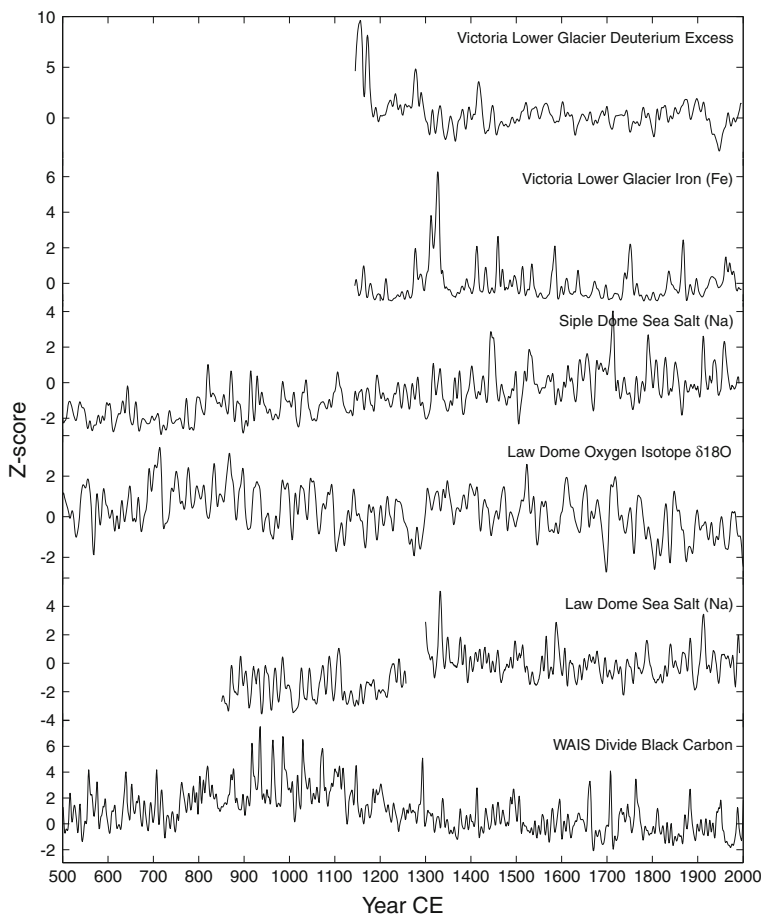
Antarctic ice core records of stable isotope ($\delta^{18}\text{O}$, δD), major ion glaciochemistry, and black carbon) at Law Dome (DSS, S66°, E112°), Siple Dome (SD, S81°, E212°), Victoria Lower Glacier (VLG, S77.2°, E166.5°), WAIS Divide (S79.3°, E248°) and EPICA Dronning Maud Land (S75°, E0.5°) have been resolved at high temporal (quasi-monthly, annual to biennial) resolution, using multiple volcanic chronological tie points in addition to seasonal/annual stratigraphic layering. Hence, the time series are robustly controlled and have been published as proxies for surface or lower tropospheric atmospheric circulation (Kreutz et al. 2000; Goodwin et al. 2004; Mayewski et al. 2004; Moy Australian Antarctic Division, pers. comm. 2011; Bertler et al. 2011). We examined a suite of these proxies for the identification of climate shifts during the SH-MCA. Six of the ice core time series are shown in Fig. 2, and described below:

- The DSS $\delta^{18}\text{O}$ record is a proxy for SLP anomalies in the south eastern Indian Ocean and Southern Ocean sector between 100° and 130° E, where warm (cool) $\delta^{18}\text{O}$ represent northerly (westerly) wind anomalies over the Southern Ocean associated with poleward

(equatorward) sub-tropical ridge south of Western Australia associated with La Niña (El Niño) and +ve (−ve) SAM phases (Delmotte et al. 2000; van Ommen and Morgan 2010).

- The DSS sodium sea-salt aerosol (Na) record for May–June–July (MJJ) is a proxy for SLPa in the south western Pacific Ocean and mid-latitude Southern Ocean sector between 150° and 170° S, where high (low) Na represents full circumpolar trough (shallow trough, poleward), low pressure anomalies over the Southern Ocean associated with PSA2−ve (PSA2+ve) and −ve (+ve) SAM phases (Goodwin et al. 2004).
- The VLG Deuterium Excess record and Iron concentration record are proxies for wind fields over the Ross Sea and northern Victoria Land mountains, respectively (Bertler et al. 2011).
- The SD sea-salt sodium aerosol (Na) record is a proxy for SLPa in the Central to Eastern south Pacific and Amundsen Sea region in the South Pacific between 200° and 270° S, where high (low) Na represents a strengthened (weakened) polar vortex associated with PSA1−ve (PSA1+ve) and +ve (−ve) SAM phases (Kreutz et al. 2000). The SD Na record is most sensitive to circulation anomalies during SON.

Fig. 2 Time series stack of ice core proxies from East and West Antarctica shown as 20 year running average values. The glaciochemical or isotope anomalies are shown against Z-scores, to illustrate the intervals of anomalous regional climate compared to the long-term millennial mean climate (1300–2000 CE). The references for the time series are listed in Table 1 and in the text



Sedimentary records also contain information on shifts in hydrological balance. The McMurdo Dry Valley lakes (Lake Fryxell and Lake Hoare) along the western Ross Sea coast in Victoria Land indicate that these lakes lost their perennial ice cover and were desiccated prior to ~ 1000 CE by low meltwater inflows, low humidity and evaporative loss (Lyons et al. 1998). Recent research by Speirs et al. (2010) indicates that foehn winds associated with ridging over Victoria Land cause relatively warm air to drain down the Dry Valleys, elevating the temperature by ~ 20 °C, and results in a negative hydrological balance. Hall et al. (2010) reported a reduced glacial ice extent along the western Antarctic Peninsula between 980 and 1250 CE that they attributed to a regional climate warming. The reduced ice extent was comparable to the observed changes in the late twentieth century.

2.2 Eastern Australia

Eastern Australian coastal strandplains contain a sedimentary and geomorphic record of the evolution of wind field changes in the Coral and Tasman Seas, and Southern Ocean, through wave climate shifts in both energy and direction. The impact of nearshore wave climate and wave-driven longshore sand transport variability is preserved at multi-decadal resolution in the successive orientation and curvature of the coastline planform (Goodwin et al. 2006). The modal wave climate is a function of the latitude of the Subtropical Ridge (STR) and hence, is sensitive to changes in the contribution of waves generated from trade winds and/or extratropical cyclones that enter the Southern Tasman/Southern Ocean (Goodwin 2005). The strandplain record extends from Fraser Island in SE Queensland to the mid-North Coast NSW. The coastline experienced an anti-clockwise realignment in response to increased ESE tradewind generated sea and swell between 600 and ~ 1000 CE (Goodwin et al. 2006). Strandplains at Keppel Bay, in central Queensland show elevated fluvial sediment discharge from 500 to 1000 CE in response to increased tropical flooding (Brooke et al. 2008). Southern NSW coastal river valleys such as the Shoalhaven experienced persistent flooding between 750 and ~ 1000 CE. Onshore sand supply increased and estuarine entrance recurved spits occurred from 1000 to ~ 1350 CE with an increase in wave energy from the ESE associated with an interpreted increase in SE trades, Central Tasman Lows and East Coast Cyclone wave energy. There is evidence from some back barrier estuaries for a transition from marine to brackish hydrology post 1000 CE (Mettam et al. 2011), probably in response to the high rates of onshore sand transport and entrance closure. Fraser Island sediment cores record an increase in rainforest vegetation pollen (Donders et al. 2006) that reflects an increase in the onshore moisture flux

during this period. Post ~ 1350 CE longer period and lower wave energy from the Southern Tasman Sea region drove progradation and clockwise rotation of the coastline, in conjunction with persistent longshore sand transport.

2.3 Southern Australia

Southern Australian playa lakes in the semi-arid zone, marr-lakes and cave drainage systems are sensitive recorders of hydrological shifts associated with Southern Ocean frontal rainfall, continental lows, inland troughs and most important the latitude of the sub-tropical ridge and the amplitude of the atmospheric longwave, steering extratropical lows. Sedimentary and geomorphic evidence from Lake Frome—Callabonna (in the Central Australian arid region) reveals that prior to ~ 1000 CE a playa-lake highstand existed (Cohen et al. 2011, 2012), that indicates lake filling from an increase in rainfall from Southern Ocean/Continental lows/Cut-off lows (after Risbey et al. 2009) relative to lake inflows from remote tropical lows. Williams et al. (2010) reported that during this pluvial period the Australian Aboriginal population in southern Central Australia was sedentary, rather than nomadic post ~ 1100 CE. Further south-east, marr-lakes such as Lake Surprise in western Victoria, record a transition from dry to wet at 1000 CE (Barr 2010), which indicates an eastwards shift in the longwave trough over SE Australia post 1000 CE. Preliminary results from oxygen isotope analysis on speleothems from southwest Western Australia suggest dry conditions prior to ~ 1370 CE (P. Treble, ANSTO pers. comm. 2011) that are known to occur when the longwave ridge persists over the eastern Indian Ocean (Allan and Haylock 1993).

2.4 New Zealand, South West Pacific Islands and sub Antarctic Islands (Pacific sector)

Lorrey et al. (2007, 2008) compiled a synthesis of proxy records for New Zealand that included tree ring, speleothem, lacustrine, pollen and glaciocedimentary climate interpretations. They integrated the proxy climate signals via a regional climate regime classification (RCRC) approach. That technique interpreted the heterogeneous spatial patterns seen in the proxy signals in terms of synoptic type frequency changes for discrete time periods. It relies heavily on the fact that circulation anomalies generate incident flow directions that interact with prominent axial ranges on both major islands to cause distinct orographic precipitation patterns. At ~ 1050 – 1200 CE Lorrey et al. (2008) attributed a relatively warm period (but spatially heterogeneous) to increased frequency of ‘blocking’ circulation patterns (following Kidson 2000), which are typified by an easterly and north-easterly wind flow over

New Zealand. That inference was based on the distribution of interpreted precipitation anomalies [a wet Eastern North Island (ENI), and dry West South Island (WSI)] and is more typical of what occurs during La Niña years and/or IPO—periods (often in conjunction with +ve SAM). They also interpreted a period of zonal southwesterly flow during 1250–1350 CE from dry ENI and wet WSI anomalies. That ‘zonal’ pattern, which includes evidence of Southern Alps glacial advances (Schaefer et al. 2009), is generally associated with positive SLPa over Australia and negative MSLP anomalies over French Polynesia during austral summer, typical of an El Niño and/or IPO+ phases (and reinforced by –ve SAM conditions).

Further north speleothem records from the south coast of Viti Levu in Fiji record an abrupt drying in the 1200’s CE (Mattey et al. 2011). That climate pattern indicates high moisture flux from increased easterly trade wind flow prior to ~1200 AD. In the subtropical southern Cook Islands (Rarotonga) low relative sea-level anomalies were coupled to cool SSTa from 950 to 1000 CE (Goodwin and Harvey 2008). Equivalent cool SSTa in the modern instrumental record occur during periods of strong water mass advection northwards from the subtropical convergence.

2.5 Patagonian South America, sub-Antarctic Islands (Atlantic sector)

The climate of Patagonian South America is sensitive to both latitudinal and longitudinal shifts in the extratropical longwave pattern, as shown by the regional synoptic typing by Aravena and Luckman (2008). There are several proxy records of air temperature, SSTa, lake hydrology and precipitation that contain information about the MCA. Moy et al. (2008) reported proxy water balance record from Lake Guanaco in Southern Patagonia, with low (high) evaporation rates in conjunction with reduced (increased) westerly winds prior to 1100 CE (1100–1300 CE) stages of the MCA. Mohtadi et al. (2007) interpreted a cool SSTa in the continental slope waters off southern Chilean Patagonia between 700 and 1250 CE, which indicates a northward shift in the advection of water from the Antarctic Circumpolar Current. Neukom et al. (2010) produced a multi-proxy reconstruction of summer and winter air temperatures over Patagonia. The reconstruction indicates that warm summer temperature anomalies characterized the period from 1150 to 1350 CE.

Subantarctic lake sediment records from the South Orkney Islands and South Georgia, (Rosqvist et al. 1999; Noon et al. 2003) record warm and dry anomalies in association with open water rather than sea-ice cover in summer between 1080 and 1280 CE, followed by a cold event and glacial readvance at ~1350 CE.

2.6 Southern and Eastern Africa

Both terrestrial and marine proxy evidence for climate anomalies in southern Africa during the MCA are scant, and only a few time series are available. In western South Africa, oxygen isotopes for estuarine mollusk shells (proxy SST) from Elands Bay (Cohen et al. 1992; Tyson and Lindesay 1992) and estuarine diatom assemblages (proxy salinity and rainfall) from Verlorenvlei, Elands Bay (Stager et al. 2012) indicate that western South Africa was dry with warm coastal SST. In eastern South Africa, cave speleothem grey scale (proxy rainfall) from Makapansgat Valley (Holmgren et al. 1999; Lee-Thorp et al. 2001), and lake diatom assemblages from Lake Nhaucati in Mozambique (Ekblom and Stabel 2008) indicate dry anomalies 700–800 CE, wet anomalies 800–900 CE, a mix of wet and dry anomalies from 900 to 1450 CE, and wet anomalies to 1550 CE.

Further north, in tropical East Africa, lake sediment records from Lake Tanganyika, in Tanzania, include proxy lake surface water temperature and charcoal record (proxy fire and aridity record) and lake diatom records (Stager et al. 2009; Tierney et al. 2010b). These indicate cooler surface water temperatures, wetter and high fire frequency prior to ~1100 CE, followed by warm surface water temperatures, and more dry arid conditions and low fire frequency to 1400 CE. This is in agreement with the Lake Victoria proxy rainfall record (Mayewski et al. 2004; Stager et al. 2005, 2007).

2.7 Overview of proxy evidence and multi-decadal to centennial variability during the MCA

The regional summaries of available proxy climate data include both continuous time series and discrete chronological point data. The data contain the regional climate impacts associated with poleward/equatorward state changes in the subtropical anticyclone and jet, extratropical westerly track and amplitude of the longwave. The collection of SH proxy climate records define a two-stage MCA associated with a distinct shift in mean climate state between: (1) 800 to ~1100 CE, and (2) ~1100 to 1300 CE. The data also describe an abrupt end to the SH MCA at ~1280 to 1300 CE with a shift in mean state. This is particularly evident in the SD and Law Dome proxy SLP records. We have sub-divided the MCA into multi-decadal to centennial epochs, based on the contemporaneous proxy climate shifts, the spatial coverage and chronological resolution of the proxy data. Accordingly, we reconstruct the circulation anomalies for 800–900 CE, 900–1000 CE, 1000–1100 CE, 1100–1150 CE, 1150–1220 CE, 1220–1300 CE, 1300–1350 CE, 1350–1400 CE and 1400–1450 CE.

3 Methodology for the reconstruction of southern hemisphere circulation anomalies

3.1 Overview of methodology

Atmospheric circulation (SLPa) and mean climate state fields are reconstructed for the above periods during the MCA by selecting climate states from an AOGCM simulation that are analogous to palaeoclimate states inferred from a multivariate suite of SH proxy records. The methodology is based on established techniques (Goosse et al. 2006; Graham et al. 2007). Analogue-based methods have been shown to accurately reconstruct spatial fields across a range of timescales and are highly flexible in terms of input data (Goosse et al. 2006; Graham et al. 2007; Trouet et al. 2009; Büntgen et al. 2010; Luterbacher et al. 2010; Franke et al. 2010; Schenk and Zorita 2012). As the cross-spatial and cross-variable relationships inherent in multivariate AOGCM datasets are conserved (Graham et al. 2007), proxy records representing a range of climate variables can be used to simultaneously select analogues. In this paper, multiple climate variables were reconstructed for the discrete multidecadal time periods (as outlined above) that are defined by synchronous step changes observed across multiple proxy records. Proxy data were resampled as follows: (1) all annually-resolved data were resampled to quasi-decadal values; (2) decadal resolved data were used without resampling; and (3) discrete proxy climate data were binned to quasi-decadal values.

To facilitate the inter-comparison of multi-variate, proxy data across the SH, all decadal data were normalised to Z-scores by subtracting the long-term mean (1300–2000 CE mean) and dividing by the standard deviation. The normalised signal for each proxy was calculated from the mean of the Z-scores for each decade of a multi-decadal time slice. Z-scores were used to calculate an ordinal based descriptive classification where multidecadal means of <-0.5 (>0.5) describe extreme climate conditions and were attributed an ordinal classification of -1 ($+1$); otherwise a classification of 0 was allocated. For example a precipitation record with ordinal classifications of $+1$, 0 or -1 describe wet, mean or dry conditions respectively. Signal to noise differentiation is difficult when strong climate anomalies (Z-scores $> \pm 0.5$) do not occur. Hence, only those proxy records that record an unambiguous signal (as defined by an ordinal classification of -1 or $+1$) were included for any given multidecadal time period. The normalised values and ordinal classifications for each proxy record were combined into a vector (P) for each time period, providing a numerical summary of the paleoclimate state at that time. The composition of proxy vectors used in the analogue selection is therefore different for each time period and are shown in Fig. 3a–c.

3.2 Surrogate climate dataset

The proxy vector (P) was used to select analogues from a surrogate climate dataset. Ideally analogues should be drawn from a dataset that is as realistic to synoptic climate variability as possible. Modern reanalysis datasets, conform to modern instrumental observations, but do not contain a sufficient range of decadal, annual or seasonal climate state analogues to capture the full potential range of variability observed in the proxy records. Alternatively, AOGCM simulations are ideal for this kind of reconstruction as there is the potential to draw from an almost unlimited number of potential climate state analogues. However these analogues represent a numerical approximation of the state of the coupled atmosphere–ocean system that is only as good as the model physics parameterisation.

In this study we use a 10,000-year control simulation of natural variability from the CSIRO Mk3L climate system model version 1.2 at monthly resolution. The Mk3L model is a fully-coupled reduced-resolution global atmosphere–land-sea ice-ocean general circulation model that is designed specifically for millennial-scale climate simulations (Phipps et al. 2011). The atmospheric component of Mk3L is a computationally efficient version of the atmospheric component of the Mk3 model used in CMIP3 (Meehl et al. 2007) and the IPCC Fourth Assessment Report (Phipps et al. 2011, 2012). The model incorporates a 5.6×3.2 degree atmosphere with 18 vertical levels and a 2.8×1.6 degree ocean with 21 vertical levels; a more detailed description can be found in (Phipps et al., 2011). The 10,000-year simulation used in this study is an unforced control simulation of modern climate with constant boundary conditions; CO₂ set to 280 ppm, solar irradiance set to $1,365 \text{ W m}^{-2}$ and 1950 CE orbital parameters. The model simulates a modern day climate reasonably well including a realistic ENSO, albeit with some biases outlined in (Phipps et al. 2011). The Mk3L also produces a realistic simulation of the amplitude and spatial characteristics of the high latitude modes, the SAM, PSA1 and PSA2. EOF analysis of the Mk3L SLP data (Fig. 1) reveals the 3 leading EOF patterns are similar to those resolved from the NCEP–NCAR Reanalysis (NNR, Kalnay et al. 1996) over the 1980–2000 period (Visbeck and Hall 2004).

Initially, the synoptic controls on each proxy record over the instrumental period were identified by producing a set of 88 individual synoptic typologies for each of the multivariate proxy data from both the Mk3L model data and the NNR data. This was done to provide an insight into the sensitivity of each proxy to regional climate variations as described by both the AOGCM and NNR. For example, the Oroko Swamp tree ring records (NZ) have been interpreted

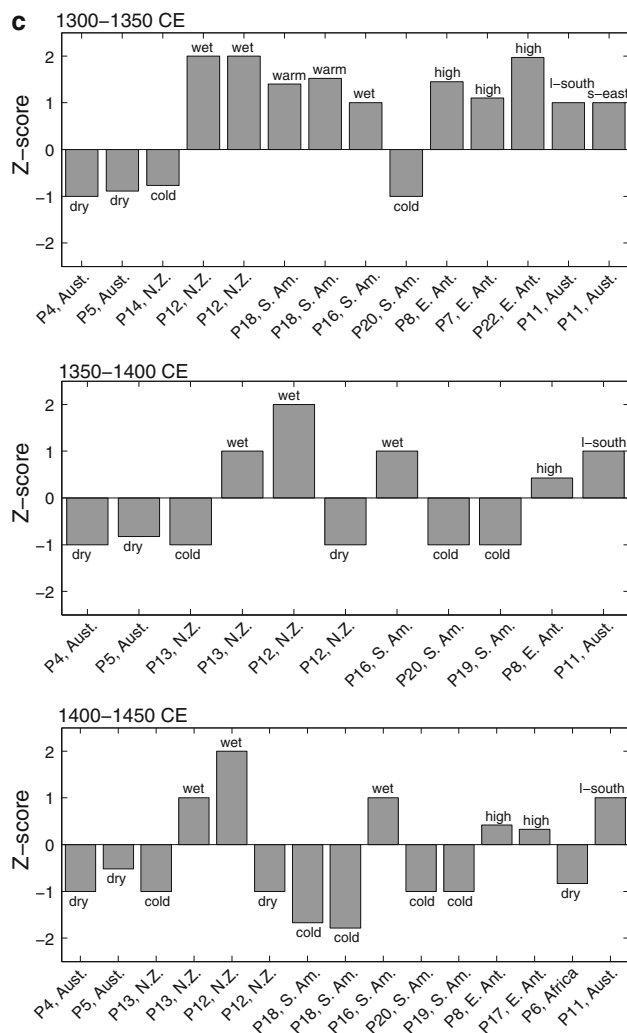


Fig. 3 continued

by the standard deviation. Each timestep was attributed an ordinal based descriptive classification. Timesteps with Z-scores of >1 (<-1) were given an ordinal classification of $+1$ (-1). All other values were given a classification of 0. Each row of S_{1-n} represents one timestep of the model dataset, with each column of S constructed as a timeseries that corresponds to the locations and variables in the proxy vector P .

3.3 Determination of best matching analogues (BMA) using evidence from multiple proxies

Modelled climate states that are analogous to the proxy inferred climate states for each discrete multidecadal time period were identified by calculating the Euclidean distance between the normalised proxy data and the normalised model data as shown in Eq. 1 (after Goosse et al. 2006):

$$D_n = \sum |P_i - S_{ni}|. \quad (1)$$

D_n is the Euclidean distance at each model timestep (n), and P is a vector (length = i) of normalised proxy values that succinctly describes the climate state for a given multi-decadal time period. Each element of P represents the normalised climate signal (pressure, temperature, wind direction, precipitation etc.) from a single proxy record or reconstruction. S is an array of timeseries (length = n) derived from the modelled climate at the equivalent geographic locations and climate variables as the elements of P . Each column of S_{1-i} corresponds to each element of P_{1-i} and each row of S_{1-n} represents one timestep of the model simulation. The Euclidean distance (D_{1-n}) is the measure of the total difference between all elements of P and S_{1-n} . Values of 0 indicate a perfect analogue while high values indicate dissimilarity. The best matching analogues (BMA) are the minima of D_{1-n} and hence are used to define the climate state for the time period of interest.

We evaluate the BMA using a concordant factor (CF), defined as the percentage of proxies (elements of P) that have the same ordinal classification as their equivalent signal each modelled timestep (D_{1-n}). We observe that there are no analogues for any time period that achieve an CF of 100 % across all proxy records. The highest CF ranges between 70 and 90 % depending on the time period. In order to ensure adequate representation of all proxies in the final reconstruction it is therefore necessary to take a mean of the BMA. Previous analogue studies have shown improvement by taking a mean of the BMA (e.g., Van den Dool 1994). However, the optimal number of BMA is not precisely determinable and is dependant on the research objectives (Mullan and Thompson 2006). Theoretically, to reconstruct climate over an n -year period, it is optimal to use the n th-number of best matching annual analogues. However, as the number of analogues contributing to the final composite are increased, the mean values of D and CF (calculated as the mean of all included analogues) tend to decrease. The standard deviation of the CF, that is a measure of the overall representation of all proxies in the final composite, decreases as more analogues are included. A set of 50 BMA was estimated to be the optimum number for: (1) including signals from all proxy records; (2) producing the highest CF; and, (3) commensurate with an equivalent multi-decadal resolution. 50 BMA also provide a large enough sample size to calculate the statistical significance and confidence intervals of all variables used in the composite analogues. Therefore, each multidecadal time period was represented by a composite analogue derived from the mean of the 50 model years that best match the multivariate suit of SH mid-latitude proxy records. Our approach to the reconstruction allows for the maintenance of cross-spatial

and cross-variable relationships in the modelled climate. This allows that any modelled variable can be interrogated. Accordingly, all modelled variables can be resolved for individual gridpoints, regions and full spatial fields for each time period (composite analogue). In reality though, only variables with a mechanistic relationship to the original proxy records should be interpreted with confidence.

3.4 Evaluation of composite analogues

The composite analogues for each time period were evaluated for consistency with proxy evidence by calculating the composite analogue values at each proxy location, using the modelled variable that corresponds to the proxy signal. Using the ordinal classifications, we also calculated the percentage of individual analogues that are concordant, discordant or neutral with regard to each proxy record. This allows the evaluation of each reconstructed time period against all original proxy signals. There are some individual records, during some time periods, which achieve a low concordant percentage. This means that the modelled climate does not contain climate states that are consistent with that signal at that location, in conjunction with all other proxy signals. This can occur because either the model does not contain the full range of possible climate states or there is some inconsistency in the dating and or interpretation of the proxy record. The effects of this problem are self limiting to a certain degree. If a proxy record is inconsistent with a physically plausible climate state that is consistent with most other proxy records, then it will not be selected in any of the BMA and will simply not contribute to the final reconstruction.

Other potential errors may arise due to: (1) dating and interpretation of proxy records; (2) limited spatial coverage of SH proxy records; (3) deficiencies in the model dataset; and, (4) potential biases in the analogue selection. For example, regions with a higher spatial representation of proxy records will be over represented at the expense of regions with limited spatial coverage, and this becomes evident when calculating the p values of the spatial SLPa composites described in Sect. 4 below. In accordance with chronological uncertainties in some of the proxy data from the early MCA, we produce centennial resolution reconstructions to minimise the potential for small errors in dating to affect the reconstructions. The reconstruction time period was shortened to ~ 50 years for the mid to late MCA. The spatial coverage of available proxy data will increase in future studies and at present the reconstructions have most confidence in the regions adjacent the locations of the proxy records. Climate state analogue deficiencies may be addressed in future studies by using a range of different AOGCM datasets. Potential biases in the analogue selection have not been addressed in this study.

Goosse et al. (2006) suggested that a weighting could be applied to each proxy record so that reconstructions favoured proxy records in which higher confidence was placed. Weighting could also be applied to reduce the effects of over representation of specific regions due to increased spatial coverage, and this will also be the subject of future work.

3.5 SLPa field reconstruction and mean climate state

Spatial mean SLP fields provide a first level explanation for the signals recorded at each proxy location, as they describe the mean circulation patterns that are likely to have dominated during the multidecadal timeslice. These circulation patterns occurred with enough persistence to leave an imprint in the environment, and are recorded in the proxy climate archives. Anomalistic SLP patterns (SLPa) were determined for each time period, relative to the 10,000 year mean SLP data. The fields were calculated using binned values for all months, and also for the Austral late autumn to spring (May to November), since the majority of available proxies were most sensitive to these months.

The SLPa patterns were compared to the EOF patterns of the leading modes of SH circulation (Fig. 1), to investigate whether statistically significant shifts in mean climate state occurred between periods. The latter for each time period was determined by calculating composite (50 BMA) values for the major modes of SH circulation. These climate index values for the 50 BMA were calculated from the full AOGCM simulation using the modern definitions: (1) ENSO (Niño3.4 SSTa) as defined by Trenberth (1997); (2) ENSO Modoki as calculated by Ashok et al. (2007); (3) IOD as calculated by Saji et al. (1999); and (4) the leading high latitude modes, SAM, PSA1 and PSA2 as calculated by Visbeck and Hall (2004). The index state for each time period was calculated as the mean (normalised to Z-scores) of the index values for all BMA in the composite analogue. Only means with $p < 0.05$ are considered to be statistically different from the long-term mean of the 10,000 year control simulation (Table 2, 3). Due to most of the proxy records being most sensitive to winter-spring season the indices were calculated for the May to November period. The derived mid to high latitude indices, SAM, PSA1 and PSA2 can be interpreted with confidence since the reconstruction and available proxies are concentrated on the extratropics. However, tropical indices such as the IOD, ENSO and ENSO Modoki derived from the modelled analogues were resolved with confidence, during periods when the low to high latitude teleconnections are active in the Indo-Pacific and are interpreted below in Sect. 4, with regard to this important caveat.

Table 2 Normalised climate index anomalies for the southern hemisphere extratropics (SAM, PSA1 and PSA2) and tropics (IOD, Niño3.4 and Modoki)

Start decade	End decade	SAM (EOF1)	PSA1 (EOF2)	PSA2 (EOF3)	Niño3.4	IOD	Modoki
800	900		0.52	0.74		-0.43	
900	1000	1.17		0.47	0.59		
1000	1100	0.95	0.74	0.34	0.91		0.75
1100	1150	0.89					
1150	1230	0.74	-0.86	-0.26	-0.40	-0.58	-0.55
1230	1300	0.73		0.75			
1300	1350	-1.55	0.70		0.46		0.26
1350	1400	-0.89	0.63	0.38	0.49	0.31	0.63
1400	1450	-0.52	0.72	0.69	0.33		

Each index was first derived from the full 10,000 year control simulation (see Sect. 3.5 for more detail). Each value in Table 2 is the normalised mean of 50 BMA; only values statistically different ($p < 0.05$) from the long term mean modelled climate (10,000 years) are shown

Table 3 The hierarchy of tropical and extratropical climate modes for each time period

Start decade	End decade	Extra-tropical 1	Extra-tropical 2	Extra-tropical 3	Tropical 1	Tropical 2	Tropical 3
800	900	PSA2+ve	PSA1+ve		IOD-ve		
900	1000	SAM+ve	PSA2+ve		El Niño		
1000	1100	SAM+ve	PSA1+ve	PSA2+ve	El Niño	CP El Niño	
1100	1150	SAM+ve					
1150	1230	PSA1-ve	SAM+ve	PSA2-ve	IOD-ve	CP La Niña	La Niña
1230	1300	PSA2+ve	SAM+ve				
1300	1350	SAM-ve	PSA1+ve		El Niño	CP El Niño	
1350	1400	SAM-ve	PSA1+ve	PSA2+ve	CP El Niño	El Niño	IOD+ve
1400	1450	PSA1+ve	PSA2+ve	SAM-ve	El Niño		

The modes for each period are ranked (1–3) by the strength of the anomaly values shown in Table 2. Only modes displaying statistically significant ($p < 0.05$) index anomalies are shown

4 Key climate features and evolution of the SH SLP patterns for each MCA time period

The reconstructed mean SLP and SLPa patterns for each time period are shown in Figs. 4, 5 derived from the CSIRO Mk3L GCM seasonal SLP data. Figure 4 shows the reconstructed SLPa patterns using all months as analogues (annual model). Figure 5 shows the reconstructed SLPa from Austral early winter to spring months (MJJASON), referred to as the winter-spring model.

The multidecadal SLPa patterns in in both the annual model and the winter-spring model depict the anomalous combinations of the leading mode (EOF1), and show changes in the annular patterns either in the Pacific, Indian or both sectors of the SH extratropics, between time periods. They also provide an insight into the more persistent higher amplitude patterns (EOF 2 and EOF 3) that contribute to the shifts in circulation, particularly in the Pacific sector between the MCA time periods. The reconstructions are limited by the potential range of circulation patterns reproduced in the model, and the model grid resolution and

topography (discussed in Sect. 3 above). In addition, the highest resolution of the EOF2 and EOF3 patterns, occurs for the time periods and regions where there is a greater spatial density of the proxy locations. The reconstruction of EOF2 and EOF3 is improved using the winter-spring model which is expected since the majority of extratropical proxies used in each time slice are most sensitive to winter or spring circulation changes. Hence, Figs. 4, 5 are interpreted and discussed together to investigate the evolution of large-scale circulation and the time-varying hierarchy of the dominant climate modes. The reconstructions revealed multicentennial persistence in circulation during 800–1100, 1100–1300, and 1300–1450. This suggests that the SH climate experiences low frequency persistence and evolution in mean climate state.

4.1 800–1100 CE

Both reconstructions show that from 800 to 1100 CE, a poleward shift in the STR is dominant with a meridional circulation pattern and a strong wave train across the

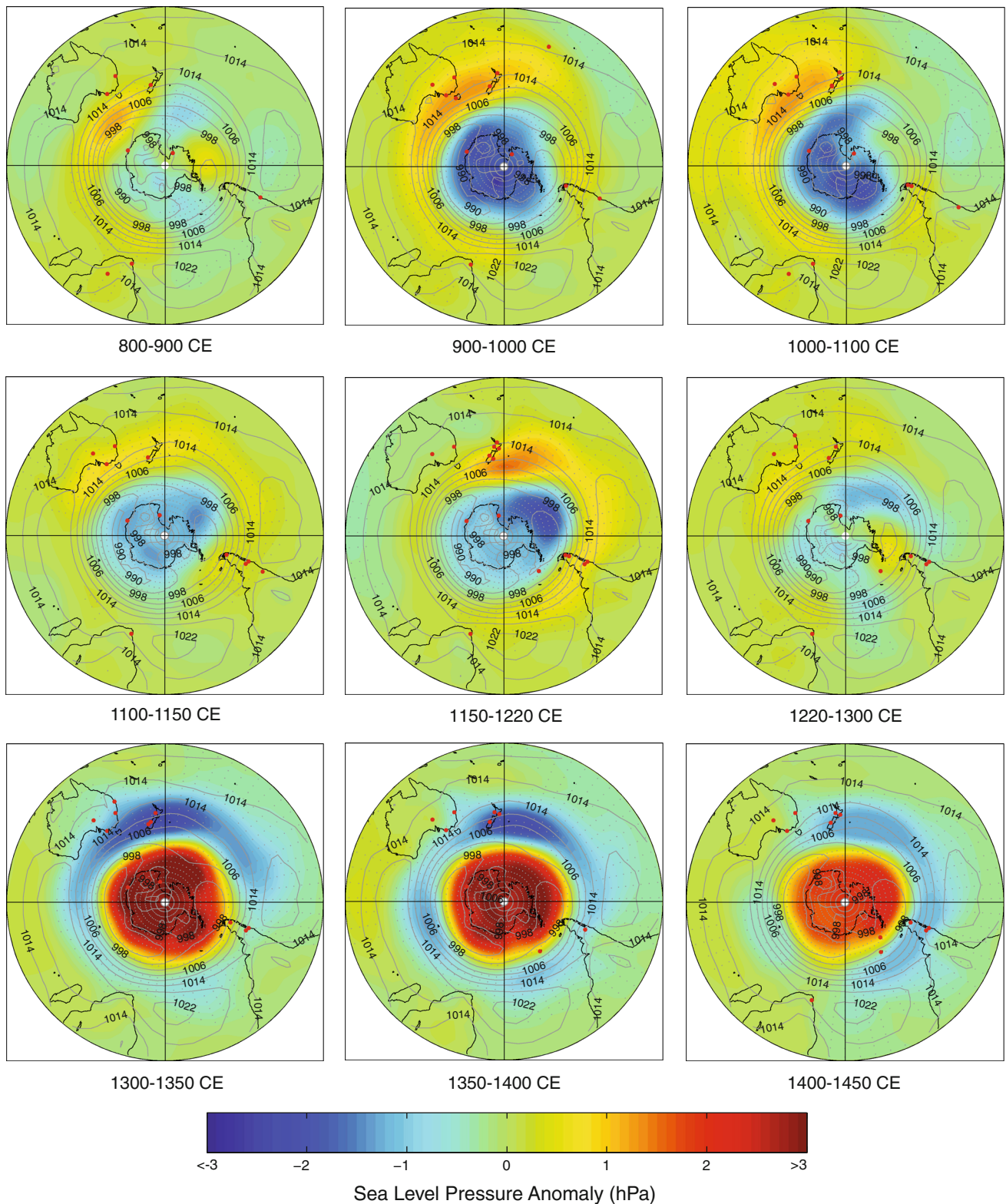


Fig. 4 Sea-level pressure mean and anomaly fields that represent the evolving mean climate states for the southern hemisphere extratropics as reconstructed from proxy climate data and 50 best matching, annual mean climate state analogues using monthly SLP output from 10,000 year runs of the CSIRO Mk3L GCM, from for the epochs:

700–900 CE, 900–1000 CE, 1000–1100 CE, 1100–1150 CE, 1150–1220 CE, 1220–1300 CE, 1300–1350 CE, 1350–1400 CE and 1400–1450 CE. The *stippling* in each figure defines where the reconstructed SLPa is significant at the 95 % level

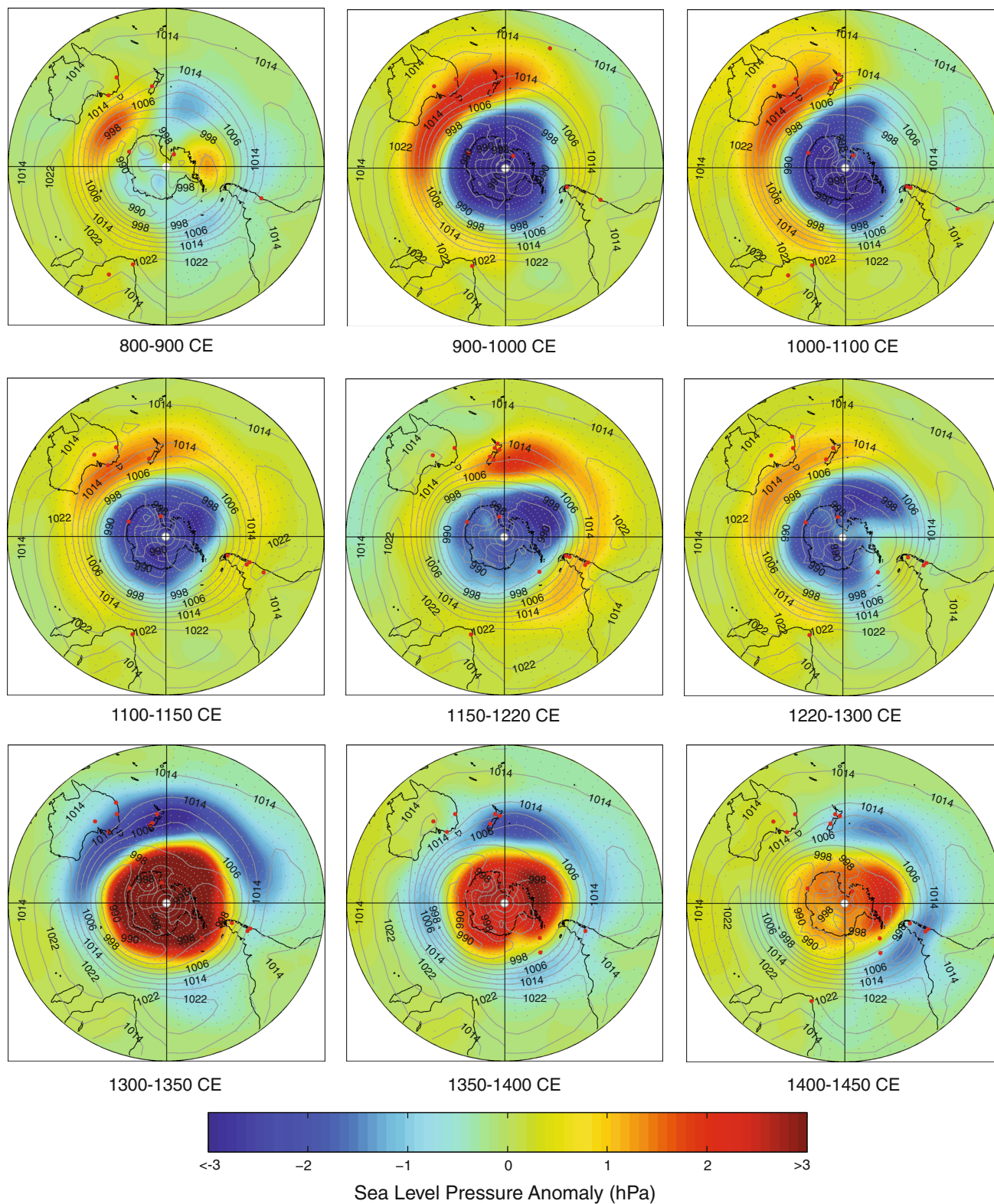


Fig. 5 Sea-level pressure anomaly fields that represent the evolving mean climate states for the southern hemisphere extratropics as reconstructed from proxy climate data and 50 best matching, Austral winter-spring mean climate state analogues using MJJASON monthly

SLP data for the epochs: 700–900 CE, 900–1000 CE, 1000–1100 CE, 1100–1150 CE, 1150–1220 CE, 1220–1300 CE, 1300–1350 CE, 1350–1400 CE and 1400–1450 CE. The *stippling* in each figure defines where the reconstructed SLPa is significant at the 95 % level

Indo-Pacific sector. The reconstructed climate mode indices indicate a dominant PSA2+ve pattern between 800 and 1000 CE, and with the SAM +ve pattern from 900 to 1100. The dominant wave pattern evolves from the PSA2+ve to PSA1+ve pattern after 1000 CE. Climatological ridges in the Tasman Sea, Amundsen Sea, western and central Indian Ocean, indicate more frequent blocking in these locations. In particular persistent blocking in the Tasman Sea region is a key interpretation during this period and is coupled to an intensification of the E–SE trade wind field in the southwest Pacific. The poleward STR is coupled to deepening of the quasi-stationary low SLPa anomalies in the Ross Sea (Pacific sector) and in the Davis Sea (Indian sector). This is consistent with observations from the instrumental era, where enhanced meridional flow into Antarctica is associated with enhanced katabatic outflow from the Lambert Glacier region and over the Ross Ice Shelf (Bromwich et al. 1993).

The region of strong positive SLPa over the Tasman Sea occurs under the PSA2+ve pattern and combined with a –ve IOD influence prior to 900 CE. This persistence of positive SLPa across the Southern Ocean south of the Tasman Sea is associated with the coupling and reinforcement of the western Pacific PSA2+ve and Indian Ocean East wave trains as seen in the modern record during SON (Cai et al. 2011a, b). This pattern is typical of the synoptic conditions for the southward passage of ex-Tropical Cyclones and a higher frequency of Easterly Trough Lows that have a subtropical origin (Browning and Goodwin 2013). The proxies during the 800–1100 period record a shift towards onshore E–SE winds and swell along the eastern Australian coast, and enhanced precipitation

along the SE Queensland and east coasts of New Zealand. Also associated with the blocking are high frequency rainfall events over southern Central Australia that caused the filling of mega-playa lakes (Cohen et al. 2012). The mega-lake filling had ceased by 1100 CE and indicates the replacement of the Southern Ocean trough with a ridge in the longwave pattern. The poleward shift in the westerlies and persistence of blocking in the eastern Pacific and western Indian Ocean explains the dry conditions over southern Patagonia (Villalba 1990) and eastern and southern South Africa (Stager et al. 2012).

4.2 1100–1300 CE

At ~1100 CE the SLPa pattern has progressed eastwards in the south-west to central Pacific sector, as shown by the shift in the location of the persistent blocking ridge from the Tasman Sea to east and south-east of New Zealand, a low SLPa in the Tasman Sea, and the progression of the low SLPa in the Ross Sea, to an strong low in the Amundsen Sea region. The blocking ridge located in the Bellingshausen Sea—Antarctic Peninsula—Chilean Patagonia region intensified during the 1100–1220 CE period. The reconstructed climate mode indices indicate an eastern Pacific or canonical La Niña PSA1–ve pattern couple to +ve SAM circulation during 1100–1150. From 1150 to 1230, the eastern Pacific PSA1–ve pattern is replaced by a Central Pacific (CP) or Modoki pattern, coupled to the persistent +ve SAM pattern. We have few modern observations of this pattern. The most appropriate SLPa examples are the NCEP SLPa composite anomalies for 1983 and 1998 SON seasons (Fig. 6) when CP La Niña events

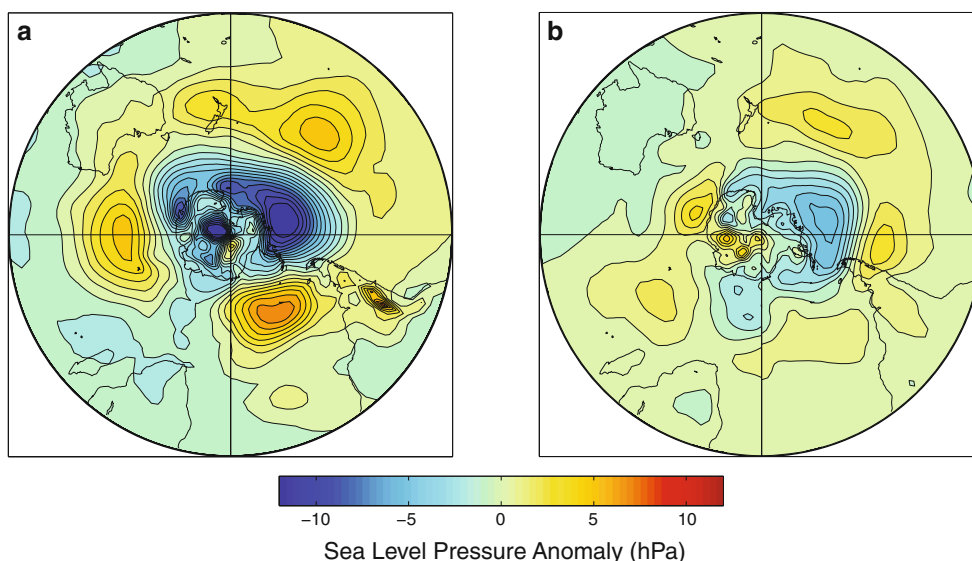


Fig. 6 SLPa composites for SON to show the rotation of the mid-latitude high pressure anomalies in the Pacific sector associated with +ve SAM combined with (a) strong EP La Niña years in 2008 and 2010; in contrast to (b) strong CP La Niña or Modoki years in 1983 and 1998

occurred (Kalnay et al. 1996; Ashok et al. 2007) in conjunction with a +ve SAM. Also shown for comparison are the equivalent SLPa composite patterns for strong EP La Niña events and +ve SAM in 2008 and 2010. The key differences in the CP composite are the westward rotation and intensification of the high SLPa to the east of New Zealand and west of Chilean Patagonia. Over Antarctica, the asymmetric zonal circulation pattern (centred on the Amundsen Sea) is characteristic of a +ve SAM and the rotated PSA1 pattern.

The climate pattern during the 1150–1220 CE period defines significant synoptic conditions for extreme weather along the Eastern Australian seaboard. The trough in the central Tasman Sea extending into the subtropical Coral Sea is cradled by a high pressure ridge over southeast Australia and the southern Tasman Sea, towards Antarctica, and is usually associated with a strengthened subtropical jet. This blocking pattern is the synoptic type related to mid-latitude Southern Secondary Lows that are cut off from the westerlies, and occur at the confluence of warm airmasses from the north-east Indian Ocean and the south-west Pacific Ocean (Hopkins and Holland 1997; Browning and Goodwin 2013).

The 1220–1300 CE period marks a major change in the asymmetry of the SAM associated with a shift in the intensity of the STR in the Indian Ocean sector, in combination with the shift from PSA1–ve to PSA2+ve pattern. The Pacific sector shows a weakening of low SLPa in the Amundsen Sea and a poleward migration of the high SLPa into the Bellingshausen Sea—Antarctic Peninsula region. In the eastern Pacific, strengthened mid-latitude westerlies re-established and this is reflected in the increased precipitation over Southern Patagonia (Villalba 1990). During the 1220–1300 CE period, some of the Pacific and Antarctic proxies record an abrupt shift in regional temperature, precipitation and winds, such as New Zealand tree rings, SD, Law Dome and the VLG ice core glaciocchemistry, and Patagonian lake hydrology. Our reconstruction identifies that these climate change impacts are associated with an abrupt shift in the SAM state from positive to negative around 1280–1300 CE.

4.3 1300–1450 CE

Following multi-centennial persistence, both the tropical and extratropical modes post 1300 CE describe a shift in mean climate state to –ve SAM coupled to a El Niño-like mean state. The equatorward shift in the westerly track and a strengthening of high pressure over Antarctica post 1300 CE is associated with the shift to dominant –ve SAM circulation previously identified by Goodwin et al. (2004). An equatorward shift in the STR and strengthening zonal mid-latitude westerlies are a characteristic in the central to

eastern Pacific and the Indian Ocean sector. The post 1300 CE dominance of the PSA1+ve mode (and strengthening CP pattern) indicates a shift towards a more El Niño-like mean state and is consistent with the multi-centennial ENSO reconstruction from New Zealand tree rings by Fowler et al. (2012) who reported persistent ENSO activity (and a strong ENSO teleconnection to New Zealand) during 1300–1400 CE, equivalent or higher than in recent decades.

The circulation post 1300, indicates a deepening of mid-latitude lows in the Southern Tasman Sea and New Zealand, eastern Pacific, and South Atlantic sectors. The climatological low in the Tasman Sea region would be associated with an increased frequency of westerly and southerly (disturbed) flow into New Zealand. That synoptic situation would help to generate the positive (negative) precipitation (temperature) anomalies interpreted in proxies across the western South Island of New Zealand. Those types of regional climate anomalies, driven by circulation, are also supported by evidence of glacial advances during the early to mid- 2nd Millennium CE (summarized in Lorrey et al. 2008, 2013, and demonstrated in Schaefer et al. 2009; Putnam et al. 2012). From 1350 CE, the westerlies were weakened in the Australian sector, with the establishment of a strengthened high pressure ridge. Contemporaneously, south–east Australia experienced a drying trend (Barr 2010), and the east coast of Australia experienced a trend to longer period SSE wave climate generated by the Southern Tasman Lows. This trend is recorded in ~200 years of coastline progradation, and the sedimentary evidence suggests a quiescent storm period (Goodwin et al. 2006). In Southern Patagonia the return to zonal westerly airflow drove an increase in precipitation and may explain the coastal oceanographic changes identified in Mohtadi et al. (2007) associated with the advection of warmer and saltier surface water along the Chilean coast.

5 Discussion on the interaction of SAM, and PSA modes and non-stationarity of tropical-extratropical teleconnections

In this section we investigate the evolution of climate modes and the non-stationarity of Indo-Pacific mid-latitude to extratropical teleconnection patterns. As a starting point we have summarized the mean climate states and changes in the location of the STR, the westerlies and mid-latitude blocking centres during the MCA in cartoon format in Fig. 7.

5.1 SAM and subtropical ridge variability

During the MCA, the SAM was shifted towards its high or positive phase with a poleward STR, and post 1300 CE

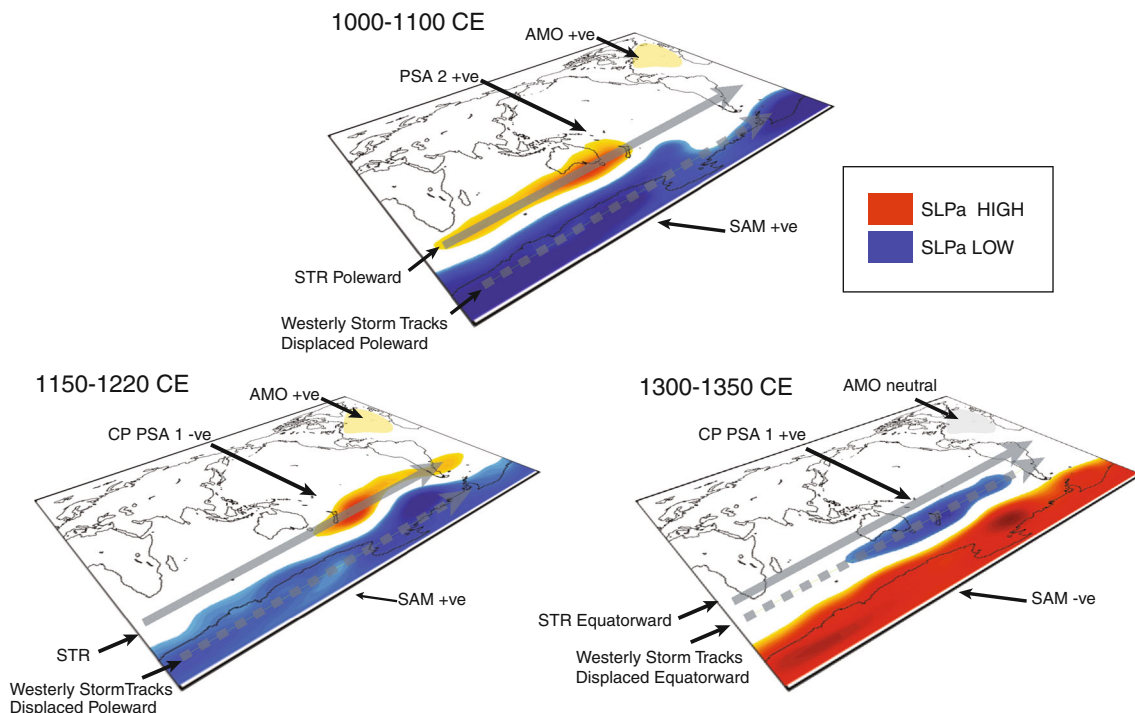


Fig. 7 Cartoon showing the subtropical to extratropical large-scale atmospheric circulation anomalies and mean climate states for the key epochs of the MCA. Also shown are the interpreted latitudinal shifts

in the Subtropical Ridge, and the Westerly storm tracks, together with the longitudinal shifts in the regions of high SLPa that represent persistent mid-latitude blocking locations

during the MCA–LIA transition this was abruptly replaced to a strong low or –ve phase with an equatorward STR. The post 1300 CE shift in the SAM towards strengthened mid-latitude westerlies (40°–50°S), supports Rodgers et al. (2011), who examined the Southern Ocean surface (10 m) wind speeds from the interhemispheric gradient in the mixing of atmospheric radiocarbon ($\Delta^{14}\text{C}$) from mid-latitude tree ring data. They interpreted that multi-decadal mean Southern Ocean zonal wind speeds were strongest during the 1275–1375 CE period, than those during the past 600 years. We interpret a deepening trough and strengthened Southern Ocean wind field at ~45 to 55°S during the 1300–1400 CE period with the shift to –ve SAM anomalies in association with an equatorward shift in the westerly storm tracks. The strongest wind field occurs over the Southern Ocean and South Pacific, and is adjacent to the tree ring records (Tasmania, New Zealand and Patagonia) included in Rodgers et al. (2011).

The interaction between the SAM and the Hadley Circulation results in the temporal behavior in both the latitude and intensity of the STR (Cai et al. 2011a), and together with the PSA phases controls the location of persistent ridging in the extratropical longwave and associated synoptic-scale blocking, particularly in the Southern Australian, Tasman Sea or east of New Zealand locations and the eastern Pacific (Chilean Patagonia, Bellingshausen Sea,

Antarctic Peninsula). The archive of very prominent proxy hydroclimate signals both in the mid-latitudes and Antarctica during the MCA is testament to anomalously frequent synoptic-scale blocking, in association with the poleward position of the STR. Wave trains emanating from the Indian Ocean convective centres associated with the Indian Ocean Dipole (IOD) have been shown to play an important role in the construction or destruction of blocking anomalies associated with ENSO phases in the Australian region (Cai et al. 2011a). The MCA SLPa patterns show contrasting patterns of ridging with the combination of poleward STR and extratropical ridging in the Indian Ocean sector during 900–1000 CE and shifted to the Pacific Ocean sector during 1150–1230 CE. Cai et al. (2011b) showed that large-scale shifts in STR intensity are related to tropical-extratropical wave train interaction. They established for the modern SON seasons, that blocking located in the Tasman Sea and over the Southern Ocean, south of Australia, such as during 800–1100, was associated with constructive wave train interaction from the eastern Indian Ocean and south-west Pacific Ocean during coupled IOD +ve and El Niño phases. Accordingly, STR position and blocking intensity located east of New Zealand, such as during 1150–1220 CE is associated with wave train interaction under +ve SAM and La Niña phases (after Cai et al. 2011a, b), and strengthened during the CP La Niña.

5.2 Tropical: extratropical interactions

Tropical-extratropical connections have been a key focus in understanding decadal variability associated with the PDO/IPO and SAM, the relationship between ENSO and the Antarctic, and resulting decadal variability in moisture and heat transport, and sea ice extent and concentration. Whilst the PSA modes are known to influence SH climate at intraseasonal, interannual and decadal time scales (Kiladis and Mo 1998; Mo and Higgins 1998), our MCA SLPa reconstruction shows that on longer time scales (multi-decades to centuries), the leading PSA mode varies also. We determined that the PSA2+ve (El Niño-like) was the more dominant mode from ~800 to 1000 CE, PSA1+ve (El Niño-like) from 1000 to 1100 CE, CP PSA1–ve (La Niña-like) from 1100 to 1220 CE, PSA2+ve (El Niño-like) from 1230 to 1300 CE, and was replaced by the CP PSA1+ve (El Niño-like) mode from 1300 to 1400 CE.

Turner (2004) concluded that the tropical ENSO signal was transmitted via the PSA wave train to the Antarctic, and L'Hereux and Thompson (2006) reported a linear relationship between the SAM and ENSO. However, the short instrumental record has thwarted a detailed investigation into the temporal relationship between the ENSO signal and the SAM (such as Fogt and Bromwich 2006; Fogt et al. 2011). The mid-latitude coupling of the climate modes is strongest during +ve SAM and La Niña phases, and –ve SAM and El Niño phases, and causes strong transmission of the ENSO signal across the South Pacific to Antarctica, due to the reinforcement of circulation anomalies by transient eddy momentum fluxes Fogt et al. (2011).

The SAM vacillations in the Pacific sector are partly forced by central Pacific SST variability (Ding et al. 2012), which in turn influences West Antarctic temperature. Ding et al. (2011) found in the late twentieth century that anomalous JJA and SON warming in the ABS and West Antarctica occurred in association with PSA (1+ve and 2+ve) atmospheric wave trains travelling from the CP equatorial region and in the western Pacific, South Pacific Convergence Zone region. Steig et al. (2013) reported that this tropical forcing was associated with West Antarctic warming, reduced sea-ice concentration in the Amundsen Sea and shelf incursions of warm Circumpolar Deep Water during the 1940's and 1990's. Steig et al. (2013) show that such conditions in West Antarctica have a strong decadal-multidecadal variability over the past 2000 years.

The SLPa reconstruction during the MCA indicates a strong tropical forcing of Antarctic climate, prior to 1100 CE. Our reconstruction shows a persistence of the PSA2+ve pattern coupled to a poleward STR in the Indian Ocean and SW Pacific Ocean sectors, during the 800–1100 CE period and we conclude that anomalous warming occurred in both West and East Antarctica during this

period due to the enhanced meridional heat transport into Wilkes Land, Victoria Land and Marie Byrd Land. Borehole temperature reconstructions from the WAIS Divide site in West Antarctica (Orsi et al. 2012) support this conclusion, and reveals surface temperatures warmer than the 1950–1980 period. Similarly, $\delta^{18}\text{O}$ time series from DSS (shown in Fig. 2) reveal that proxy surface temperatures in Wilkes Land were anomalously warm during the 800–1000 CE period. The shift to –ve SAM and CP PSA1–ve (La Niña) modes during 1200–1300 CE is contemporaneous with anomalous cooling across Antarctica (PAGES 2K network, 2013). Our SLPa reconstruction supports Steig et al. (2013) that the recent tropical forcing of warming in West Antarctica over the past 50 years may not be unique, and was persistent during the early MCA and contemporaneous with Northern Hemisphere warming during the AMO+ve climate mode.

A significant shift in the multi-decadal mean state from +ve SAM/La Niña-like to –ve SAM/El Niño-like occurred at ~1280 to 1300 CE. This abrupt shift conforms to the Tsonis et al. (2007) findings that synchronicity between the tropics and extratropics ends abruptly with a phase shift or flip in mean climate state, such as the 1976/77 Pacific climate shift (Miller et al. 1994). In the 800–1100 CE period, the strongest tropical link with Antarctica originated in the Indian Ocean and western Pacific, under the dominance of the PSA 2 and is characteristic of JJA and SON seasons in the late twentieth century (Ding et al. 2012). In the latter period from 1300 to 1450 CE, when the PSA 1 dominates, the strongest tropical link to Antarctica is via the central to eastern Pacific that is characteristic of DJF seasons in the late twentieth century (Ding et al. 2012). Also associated with the mean climate shift at ~1300 CE, are the strongest hydroclimate, wave climate and wind field signals in the south-eastern Australian/NZ sector, that are associated with both the CP La Niña phase from 1150 to 1220 CE, and the CP El Niño phase from 1350 to 1400 CE.

5.3 Non-stationarity of Indo-Pacific teleconnection patterns with the Amundsen Sea and West Antarctica

Analyses of the influence of the central Pacific on the climate of West Antarctica during the instrumental era, (examples referred to above by Ding et al. 2011, 2012), together with other studies of ENSO influences on Antarctica rely on a quasi stationary dipole between the Central Pacific and West Antarctica. Our SLPa reconstruction highlights a possible non-stationarity in the 'atmospheric bridge' teleconnection between the SLP field over the ABS region and the tropical Indo-Pacific. Coupled to the low-frequency SAM evolution are time-varying annulus

asymmetries: (1) in the Ross Sea and Central Pacific sector during 800–1100 CE; (2) in the Amundsen Sea during 1100–1300 CE; and, (3) in the Ross Sea and Davis Sea sectors during 1300–1450 CE. These asymmetries can be interpreted as the extratropical interaction of persistent wave trains emanating from the tropics and mid-latitudes that are diagnostic of the PSA modes. In contrast, the variability in the Indian sector is maintained by a meridional dipole in pressure centered on 80°–100°E between the mid-latitudes and East Antarctica, that is also observed in the late twentieth century (Ding et al. 2012).

In observational data, El Niño (La Niña) phases have been related to positive (negative) SLPa in the ABS region (Karoly 1989), and the SAM exhibits an asymmetry in this sector under both phases of ENSO (Fogt and Bromwich 2006, Fogt et al. 2011). However, during the MCA our reconstruction shows that positive SLPa in the ABS region are a persistent feature despite PSA mode changes, e.g., 800–1100, 1100–1230, and 1300–1450 CE. Higher wave number circulation in the extratropical Indo-Pacific complicates the teleconnection relationships between the tropical and mid-latitude Pacific and the Ross, Amundsen and Bellingshausen Seas and Antarctic Peninsula regions.

The non-stationarity of teleconnections with the ABS region has important implications for interpreting the behaviour of the Antarctic Dipole (a see-saw pattern in Antarctic pressure, sea ice and temperature anomalies between the Amundsen Sea and the Antarctic Peninsula (Stammerjohn et al. 2008). Our reconstructions imply that during the MCA, the Antarctic Dipole was shifted westwards such that the Ross Sea and Bellingshausen Sea are the key locations with the respective warmer (colder) temperature and less (more) sea ice anomalies. Such warm temperatures in the western Ross Sea region are characteristic in the VLG ice core record of deuterium excess during 1140–1287 CE (Bertler et al. 2011) during the CP PSA1–ve and +ve SAM circulation patterns. Hence, our reconstruction suggests that the key Indo-Pacific pressure teleconnections between the extratropical and tropical eastern Indian and South Pacific Oceans may change from the Amundsen Bellingshausen Sea region to the Ross – Amundsen Sea region, depending upon persistence in tropical convection centres and the associated Indian, CP and EP wave train propagation.

6 Conclusions

The reconstructed MCA circulation pattern was developed by using a multivariate suit of proxy data to derive climate state analogues from a 10,000 year GCM simulation (CSIRO Mk3L). In the Indo-Pacific sector, the extratropical mean climate state was dominated by a strong tropical

interaction with Antarctica emanating from: (1) the eastern Indian and south-west Pacific regions prior to 1100 CE, then, (2) the eastern Pacific evolving to the central Pacific La Niña-like pattern interacting with a +ve SAM to 1300 CE. A relatively abrupt shift to –ve SAM and the central Pacific El Niño-like pattern occurred at ~1300 CE, A poleward (equatorward) shift in the STR and westerlies occurred during the MCA (MCA–LIA transition). The pressure anomalies in the extratropical South Pacific, particularly the Amundsen Sea region reflect a bipolar symmetry during the MCA with the North Atlantic region. The PSA mode evolution defined in the reconstructions supports the hypothesis of Mann et al. (2009) and Graham et al. (2010) that the mean climate state in the tropical Pacific was shifted towards more La Niña-like (El Niño-like) during the 1100–1300 (1300–1450 CE) periods.

Increased synoptic-scale blocking in the SE Australian, Tasman Sea, New Zealand and Southwest Pacific in association with the poleward shift in the STR, and extratropical ridging, is interpreted as a dominant feature of the circulation throughout the MCA. The persistence in the mid-latitude blocking is linked to the evolving hierarchy and combination of constructive/destructive interference from multiple climate phenomena (ENSO/SAM). The STR intensification and associated blocking in the SH is contemporaneous with the persistence of blocking over the north-eastern Pacific and the northern Atlantic/Southern Europe region (Graham et al. 2010). Our SH MCA reconstruction also demonstrates a bipolar symmetry in Hadley Cell expansion and poleward shift of the zonal westerlies during the MCA.

The extensive proxy climate evidence outlined in Sect. 2 that was preserved in the earth archives is testament to the persistence of meridional climate anomalies throughout the SH MCA period. Rotation of the hemispheric circulation pattern through the mid to late MCA resulted in the culmination of more frequent troughs in the central Tasman Sea and eventually over New Zealand during the late MCA. This pattern may represent the onset of the subsequent LIA in the SH.

Our results describe the multi-decadal climate impacts associated with a poleward shift in the STR during the MCA. Recent climate observations display trends in the Hadley Cell widening (Seidel et al. 2008; Vecchi et al. 2006), poleward migration in the mid-latitude storm tracks and SH jet streams, and associated changes in hydroclimate (Arblaster and Meehl 2006), that have some regional characteristics comparable to those in the MCA period. Hence, knowledge of the regional climate impacts, particularly in Australia and southwest Pacific during the MCA, may prove analogous to some of the projected climate impacts associated with the poleward shift in the STR and SW Pacific blocking under anthropogenic Greenhouse Gas and Ozone forcing this century.

Acknowledgments This work is a contribution to the PAGES2K Australasian regional synthesis (part of the PAGES Aus2k project). The research was part funded by a Macquarie University External Collaborative Grant with the News South Wales Office for Environment and Heritage, and the New South Wales Environmental Trust. The research forms a contribution to the Eastern Seaboard Climate Change Initiative (ESCCI). S. Phipps' CSIRO Mk3L modeling was supported under the Australian Research Council's Discovery Projects funding scheme (Project Number DP1092945). AML was supported in part by the NIWA core-funded project "Climate Present and Past". The paper draws on a significant proxy climate database interpreted from Antarctic Ice Coring and we acknowledge the support of the US National Science Foundation Office of Polar Programs, Antarctica New Zealand and the Australian Antarctic Division. We thank the reviewers for their constructive suggestions to improve both the methodology and manuscript.

References

- Allan RJ, Haylock MR (1993) Circulation features associated with the winter rainfall decrease in southwestern Australia. *J Clim* 6:1356–1367
- Aravena JC, Luckman BH (2008) Spatio-temporal rainfall patterns in Southern South America. *Int J Climatol*. doi:10.1002/joc.1761
- Arblaster J, Meehl G (2006) Contributions of external forcings to southern annular mode trends. *J Clim* 19:2896–2905
- Ashok K, Behera S, Rao S, Weng H, Yamagata T (2007) El Niño Modoki and its possible teleconnection. *J Geophys Res* 112:C11007. doi:10.1029/2006jc003798
- Barr C (2010) Droughts and flooding rains: a fine-resolution reconstruction of climatic variability in western Victoria, Australia, over the last 1500 years. PhD thesis, University of Adelaide, Adelaide
- Bertler NAN, Mayewski PA, Carter L (2011) Cold conditions in Antarctica during the little ice age—implications for abrupt climate change mechanisms. *Earth Planet Sci Lett* 308:41–51
- Bradley RS, Hughes MK, Diaz HF (2003) Climate in medieval time. *Science* 302:404–405. doi:10.1126/science.1090372
- Bromwich DH, Carrasco JF, Liu Z, Tzeng RT (1993) Hemispheric atmospheric variations and oceanographic impacts associated with katabatic surges across the Ross Ice Shelf, Antarctica. *J Geophys Res* 98(D7):13045–13062
- Brooke B, Ryan D, Pietsch T, Olley J, Douglas G, Packett R, Radke L, Flood P (2008) Influence of climate fluctuations and changes in catchment land use on late holocene and modern beach-ridge sedimentation on a tropical macrotidal coast: Keppel Bay, Queensland, Australia. *Mar Geol* 251:195–208
- Browning S, Goodwin ID (2013) Large scale influences on the evolution of winter subtropical maritime cyclones affecting Australia's east coast. *Mon Weather Rev*. doi:10.1175/MWR-D-12-00312.1
- Büntgen U, Franke J, Frank D, Wilson R, González-Rouco F, Esper J (2010) Assessing the spatial signature of European climate reconstructions. *Clim Res* 41:125–130
- Cai W, van Rensch P, Cowan T, Hendon HH (2011a) Teleconnection pathways of ENSO and the IOD and the mechanisms for impacts on Australian rainfall. *J Clim* 24. doi:10.1175/2011JCLI4129.1
- Cai W, van Rensch P, Cowan T (2011b) Influence of global-scale variability on the subtropical ridge over southeast Australia. *J Clim* 24:6035–6053. doi:10.1175/2011JCLI4149.1
- Clement AC, Seager R, Cane MA, Zebiak SE (1996) An ocean dynamical thermostat. *J Clim* 9:2190–2196. doi:10.1175/1520-0442
- Cobb K, Charles C, Cheng H, Edwards R (2003) El Niño/Southern oscillation and tropical Pacific climate during the last millennium. *Nature* 424:271–276
- Cobb KM, Charles C, Cheng H, Edwards RL (2011) Fossil coral records of tropical Pacific climate over the last millennium: relationship to external forcing. *Proceedings of the AGU Fall Meeting, San Francisco, December, 2011*
- Cohen AL, Parkington JE, Brundrit GB, van der Merwe NJ (1992) A holocene marine climate record in mollusk shells from the southwest African coast. *Quat Res* 38:379–385
- Cohen TJ, Nanson GC, Jansen JD, Jones BG, Jacobs Z, Treble P, Price DM, May J-H, Smith AM, Ayliffe LK, Hellstrom JC et al (2011) Continental aridification and the vanishing of Australia's megalakes. *Geology* 39(2):167–170. doi:10.1130/G31518.1
- Cohen TJ, Nanson GC, Jansen JD, Gliganic LA, May J-H, Lasren L, Goodwin ID, Browning S, Price DM (2012) A pluvial episode identified in arid Australia during the medieval climatic anomaly. *Quat Sci Rev* 56:167–171. doi:10.1016/j.quascirev.2012.09.021
- Conroy JL, Overpeck JT, Cole JE, Shanahan TM, Steinitz-Kannan M (2008) Holocene changes in eastern tropical Pacific climate inferred from a Galápagos lake sediment record. *Quat Sci Rev* 27:1166–1180
- Cook E, Palmer J, D'arrigo R (2002) Evidence for a "medieval warm period" in a 1, 100 year tree-ring reconstruction of past austral summer temperatures in New Zealand. *Geophys Res Lett* 29:1667. doi:10.1029/2001gl014580
- Cook E, Buckley BM, Palmer JG, Fenwick P, Peterson MJ, Boswijk G, Fowler A et al (2006) Millennia-long tree-ring records from Tasmania and New Zealand: a basis for modelling climate variability and forcing, past, present and future. *J Quat Sci* 21: 689–699 ISSN 0267-8179
- Delmotte M, Masson V, Jouzel J, Morgan VI (2000) A seasonal deuterium excess signal at Law Dome, coastal eastern Antarctica: a southern ocean signature. *J Geophys Res* 105:7187–7197. doi:10.1029/1999jd901085
- Diaz HF, Trigo R, Hughes MK, Mann ME, Xoplaki E, Barriopedro D (2011) Spatial and temporal characteristics of climate in medieval times revisited. *Bull Am Meteorol Soc* 92:1487–1500
- Ding Q, Steig EJ, Battisti DS, Kuttel M (2011) Winter warming in West Antarctica caused by central tropical Pacific warming. *Nat Geosci* 4:398–403. doi:10.1038/ngeo1129
- Ding Q, Steig EJ, Battisti DS, Wallace JM (2012) Influence of the tropics on the southern annular mode. *J Clim* 25:6330–6348. doi:10.1175/JCLI-D-11-00523.1
- Donders TH, Wagner F, Visscher H (2006) Late pleistocene and holocene subtropical vegetation dynamics recorded in perched lake deposits on Fraser Island, Queensland, Australia. *Palaeogeogr Palaeoclimatol Palaeoecol* 241:417–439
- Eklblom A, Stabel B (2008) Paleohydrology of Lake Nhaucati (southern Mozambique), ~400 AD to present. *J Paleolimnol* 40:1127–1141
- Fogt RL, Bromwich DH (2006) Decadal variability of the ENSO teleconnection to the high-latitude South Pacific governed by coupling with the southern annular mode. *J Clim* 19:979–997
- Fogt RL, Bromwich DH, Hines KM (2011) Understanding the SAM influence on the South Pacific ENSO teleconnection. *Clim Dyn* 36:1555–1576. doi:10.1007/s00382-010-0905-0
- Folland CK, Renwick JA, Salinger MJ, Mullan B (2002) Relative influences of the the interdecadal Pacific oscillation and ENSO on the South Pacific Convergence Zone. *Geophys Res Lett* 29(13):1643. doi:10.1029/2001GL014201
- Fowler AM, Boswijk G, Lorrey AM, Gergis J, Pyrie M, McCloskey SPJ, Palmer JG, Wunder J (2012) Multi-centennial ENSO insights from New Zealand forest giants. *Nat Clim Chang*. doi:10.1038/NCLIMATE1374

- Franke J, González-Rouco JF, Frank D, Graham NE (2010) 200 Years of European temperature variability: insights from and tests of the proxy surrogate reconstruction analog method. *Clim Dyn* 37:133–150. doi:[10.1007/s00382-010-0802-6](https://doi.org/10.1007/s00382-010-0802-6)
- Goodwin ID (2005) A mid-shelf wave direction climatology for south-eastern Australia, and its relationship to the El Niño—Southern oscillation, since 1877 AD. *Int J Climatol* 25:1715–1729
- Goodwin ID, Harvey N (2008) Subtropical sea-level history from coral microatolls in the Southern Cook Islands, since 300 AD. *Mar Geol* 253:14–25
- Goodwin I, van Ommen T, Curran M, Mayewski P (2004) Mid latitude winter climate variability in the South Indian and southwest Pacific regions since 1300 AD. *Clim Dyn* 22:783–794
- Goodwin I, Stables M, Olley J (2006) Wave climate, sand budget and shoreline alignment evolution of the Iluka-Woody Bay sand barrier, northern New South Wales, Australia, since 3000 yr BP. *Mar Geol* 226:127–144
- Goosse H, Renssen H, Timmermann A, Bradley RS, Mann ME (2006) Using paleoclimate proxy-data to select optimal realisations in an ensemble of simulations of the climate of the past millennium. *Clim Dyn* 27:165–184. doi:[10.1007/s00382-006-0128-6](https://doi.org/10.1007/s00382-006-0128-6)
- Graham NE et al (2007) Tropical Pacific—mid-latitude teleconnections in medieval times. *Clim Chang* 83:241–285. doi:[10.1007/s10584-007-9239-2](https://doi.org/10.1007/s10584-007-9239-2)
- Graham NE, Ammann CM, Fleitmann D, Cobb KM, Luterbacher J (2010) Support for global climate reorganization during the “medieval climate anomaly”. *Clim Dyn*. doi:[10.1007/s00382-010-0914-z](https://doi.org/10.1007/s00382-010-0914-z)
- Griffiths ML, Kimbrough A, Gagan MK, Drysdale RN, Cole JE, Johnson KR, Zhao J-X, Hellstrom J, Ayliffe L, Hantoro W (2011) Towards an annually resolved reconstruction of Indo-Pacific hydrology over the past 2000 years. Proceedings of the AGU Fall Meeting, San Francisco, December, 2011
- Hall A, Visbeck M (2002) Synchronous variability in the southern hemisphere atmosphere, sea ice, and ocean resulting from the annular mode. *J Clim* 15:3043–3057
- Hall BL, Koffman T, Denton GH (2010) Reduced ice extent on the western Antarctic Peninsula at 700 to 970 cal Yr BP. *Geology* 38:635–638. doi:[10.1130/G309321](https://doi.org/10.1130/G309321)
- Holmgren K, Karlén W, Lauritzen SE, Lee-Thorp JA, Partridge TC, Piketh S, Repinski P, Stevenson C, Svanered O, Tyson PD (1999) 3000-Year high-resolution record of palaeoclimate for North-Eastern South Africa. *Holocene* 9(3):295–309
- Hopkins LC, Holland GJ (1997) Australian heavy-rain days and associated east coast cyclones: 1958–92. *J Clim* 10:621–635. doi:[10.1175/15200442\(1997\)010<0621:AHRDAA>2.0.CO;2](https://doi.org/10.1175/15200442(1997)010<0621:AHRDAA>2.0.CO;2)
- Jones P et al (2009) High-resolution palaeoclimatology of the last millennium: a review of current status and future prospects. *Holocene* 19:3–49
- Kalnay E et al (1996) The NCEP/NCAR 40-year reanalysis project. *Bull Am Meteorol Soc* 77:437–471
- Karoly D (1989) Southern hemisphere circulation features associated with El Niño–Southern oscillation events. *J Clim* 2:1239–1252
- Khider D, Stott LD, Emile-Geay J, Thunell R, Hammond DE (2011) Assessing El Niño oscillation variability over the past millennium. *Paleoceanography* 26:PA3222. doi:[10.1029/2011PA002139](https://doi.org/10.1029/2011PA002139)
- Kidson JW (2000) An analysis of New Zealand synoptic types and their use in defining weather regimes. *Int J Clim* 20(3):299–316
- Kiladis GN, Mo K (1998) Interannual and intraseasonal variability in the southern hemisphere. In: Karoly DJ, Vincent DG (eds) *Meteorology of the southern hemisphere*. American Meteorological Society Monograph, Boston, p 410
- Knudsen M, Seidenkrantz M-S, Jacobsen BH, Kijupers A (2011) Tracking the Atlantic multidecadal oscillation through the last 8,000 years. *Nat Commun* 2:178. doi:[10.1038/ncomms1186](https://doi.org/10.1038/ncomms1186)
- Kreutz K, Mayewski P, Pittalwala I, Meeker L, Twickler M, Whitlow S (2000) Sea level pressure variability in the Amundsen Sea region inferred from a West Antarctic glaciochemical record. *J Geophys Res* 105:4047–4059
- L’Hereux ML, Thompson DWJ (2006) Observed relationships between the El Niño–Southern oscillation and the extratropical zonal mean circulation. *J Clim* 19:276–287
- Lamb HH (1965) The early medieval warm epoch and its sequel. *Palaeogeogr Palaeoclimatol Palaeoecol* 1:13–37
- Lee-Thorp JA, Holmgren K, Lauritzen S-E, Linge H, Moberg A, Partridge TC, Stevenson C, Tyson PD (2001) Rapid climate shifts in the southern African interior throughout the mid to late holocene. *Geophys Res Lett* 28(23):4507–4510
- Linsley BK, Zhang P, Kaplan A, Howe SS, Wellington GM et al (2008) Interdecadal–decadal climate variability from multicoral oxygen isotope records in the South Pacific Convergence Zone region since 1650 AD. *Paleoceanography* 23:PA2219. doi:[10.1029/2007pa001539](https://doi.org/10.1029/2007pa001539)
- Linsley BK, Rosenthal Y, Oppo DW (2010) Holocene evolution of the Indonesian through flow and the western Pacific warm pool. *Nat Geosci* 3:578–583
- Liu Z, Alexander M (2007) Atmospheric bridge, oceanic tunnel, and global climatic teleconnections. *Rev Geophys* 45:RG2005. doi:[10.1029/2005RG000172](https://doi.org/10.1029/2005RG000172)
- Lorrey A, Fowler A, Salinger J (2007) Regional climate regime classification as a qualitative tool for interpreting multi-proxy palaeoclimate data spatial patterns: a New Zealand case study. *Palaeogeography. Palaeoclimatol Palaeoecol* 253:407–433
- Lorrey A, Williams P, Salinger J, Martin T, Palmer J, Fowler A, Zhao J-X, Neil H (2008) Speleothem stable isotope records interpreted within a multi-proxy framework and implications for New Zealand palaeoclimate reconstruction. *Quatern Int* 187:52–75
- Lorrey AM, Fauchereau N, Stanton C, Chappell PR, Phipps SJ, Mackintosh A, Renwick JA, Goodwin I, Fowler AM (2013) The Little Ice Age climate of New Zealand reconstructed from Southern Alps cirque glaciers: a synoptic type approach. *Clim Dyn*. doi:[10.1007/s00382-013-1876-8](https://doi.org/10.1007/s00382-013-1876-8)
- Luterbacher J et al (2010) Circulation dynamics and its influence on European and Mediterranean January–April climate over the past half millennium: results and insights from instrumental data, documentary evidence and coupled climate models. *Clim Chang* 101:201–234. doi:[10.1007/s10584-009-9782-0](https://doi.org/10.1007/s10584-009-9782-0)
- Lyons W, Tyler S, Wharton R Jr, McKnight D, Vaughn B et al (1998) A late holocene desiccation of Lake Hoare and Lake Fryxell, McMurdo dry Valleys, Antarctica. *Antarct Sci* 10:247–256
- MacDonald G, Case R (2005) Variations in the Pacific decadal oscillation over the past millennium. *Geophys Res Lett* 32:1–4
- Mann M, Zhang Z, Rutherford S, Bradley R, Hughes M, Shindell D, Ammann C, Faluvegi G, Ni F (2009) Global signatures and dynamical origins of the little ice age and medieval climate anomaly. *Science* 326:1256–1260. doi:[10.1126/science.1177303](https://doi.org/10.1126/science.1177303)
- Mattey D, Stephens M, Garcia_Anton E, Hoffmann D, Dredge JA, Fisher RE, Lowry D (2011) The nature of the medieval warm period—little ice age Transition in an annually resolved speleothem record from Voli Voli Cave, Fiji. Proceedings of the AGU Fall Meeting, San Francisco, December, 2011
- Mayewski PA, Rohling E, Stager JC et al (2004) Holocene climate variability. *Quat Res* 62:243–255
- Mayewski PA et al (2005) A 700 year record of southern hemisphere extratropical climate variability. *Ann Glaciol* 39:127–132
- Meehl A, Tebaldi C, Teng H, Peterson TC (2007) Current and future U.S. weather extremes and El Niño. *Geophys Res Lett* 34:L20704. doi:[10.1029/2007GL031027](https://doi.org/10.1029/2007GL031027)
- Mettam P, Tibby J, Barr C, Marshall JC (2011) Development of eighteen mile swamp, North Stradbroke Island: a palaeolimnological study. In: Arthington AH, Page TJ, Rose CW, Raghu S

- (eds) A place of sandhills: ecology, hydrogeomorphology and management of Queensland's dune islands, Proceedings of the Royal Society of Queensland, vol 117
- Miller AJ, Cayan DR, Barnett TP, Graham NE (1994) The 1976–77 climate shift of the Pacific Ocean. *Oceanography* 7:1–6
- Mo K, Higgins R (1998) The Pacific-South American modes and tropical convection during the southern hemisphere winter. *Mon Weather Rev* 126:1581–1596
- Mo K, Paegle J (2001) The Pacific-South American modes and their downstream effects. *Int J Clim* 21:1211–1229
- Mohtadi M, Romero O, Kaiser J, Hebbeln D (2007) Cooling of the southern high latitudes during the medieval period and its effect on ENSO. *Quat Sci Rev* 26:1055–1066
- Moy C, Dunbar R, Moreno P, Francois J-P, Villa-Martínez R, Mucciaroni D, Guilderson T, Garreaud R (2008) Isotopic evidence for hydrologic change related to the westerlies in SW Patagonia, Chile, during the last millennium. *Quat Sci Rev* 27:1335–1349
- Mullan AB, Thompson CS (2006) Analogue forecasting of New Zealand climate anomalies. *Int J Clim* 26(4):485–504. doi:101002/joc1261
- Neukom R et al (2010) Multiproxy summer and winter surface air temperature field reconstructions for southern South America covering the past centuries. *Clim Dyn*. doi:101007/s00382-010-0793-3
- Newton A, Thunell R, Stott L (2006) Climate and hydrographic variability in the Indo-Pacific warm pool during the last millennium. *Geophys Res Lett* 33:L19710. doi:101029/2006gl027234
- Noon PE, Leng MJ, Jones VJ (2003) Oxygen-isotope ($\delta^{18}O$) evidence of Holocene hydrological changes at Signy Island, maritime Antarctica. *Holocene* 13:251–263. doi:101191/0959683603hl611rp
- Oglesby R, Feng S, Hu Q, Rowe C (2011) The role of the Atlantic multidecadal oscillation on medieval drought in North America: synthesizing results from proxy data and climate models. *Glob Planet Chang*. doi:101016/j.globplancha201107005
- Oppo DW, Rosenthal Y, Linsley BK (2009) 2,000-Year-long temperature and hydrology reconstructions from the Indo-Pacific warm pool. *Nature* 460:1113–1116
- Orsi AJ, Cornuelle BD, Severinghaus JP (2012) Little Ice Age cold interval in West Antarctica: evidence from borehole temperature at the West Antarctic ice sheet (WAIS) divide. *Geophys Res Lett* 39:L09710. doi:10.1029/2012GL051260
- PAGES 2K network (2013) Continental-scale temperature variability during the past two millennia. *Nat Geosci*. doi:10.1038/NGEO1797
- Phipps SJ, Rotstayn LD, Gordon HB, Roberts JL, Hirst AC, Budd WF (2011) The CSIRO Mk3L climate system model version 10—part 1: description and evaluation. *Geosci Model Dev* 4:483–509. doi:105194/gmd-4-483-2011
- Phipps SJ, Rotstayn LD, Gordon HB, Roberts JL, Hirst AC, Budd WF (2012) The CSIRO Mk3L climate system model version 10—part 2: response to external forcings. *Geosci Model Dev* 5:649–682. doi:105194/gmd-5-649-2012
- Putnam AE, Schaefer JM, Denton GH, Barrell DJA, Finkel RC, Andersen BG, Schwartz R, Chinn TJC, Doughty AM (2012) Regional climate control of glaciers in New Zealand and Europe during the pre-industrial holocene. *Nat Geosci*. doi:011038/NGEO1548
- Rein B, Lückge A, Sirocko F (2004) A major holocene ENSO anomaly during the medieval period. *Geophys Res Lett* 31:L17211. doi:101029/2004gl020161
- Rein B, Lückge A, Reinhardt F, Sirocko F, Wolf A, Dullo W-C (2005) El Niño variability off Peru during the last 20,000 years. *Paleoceanography* 20:PA4003. doi:101029/2004PA001099
- Renwick JA, Revell MJ (1999) Blocking over the South Pacific and Rossby wave propagation. *Mon Weather Rev* 127:2233–2247. doi:101175/1520-0493(1999)127<2233:BOTSPA>2.0.CO;2
- Risbey JS, Pook MJ, McIntosh PC, Ummerhofer CC, Meyers G (2009) Characteristics and variability of synoptic features associated with cool season rainfall in southeastern Australia. *Int J Climatol* 29:1595–1613
- Rodgers KB et al (2011) Interhemispheric gradient of atmospheric radiocarbon reveals natural variability of Southern Ocean winds. *Clim Past Discuss* 7:347–379
- Rodysill JR, Russell JM, Bijaksana S, Brown E, Safiuddin L, Eggermont H et al (2011) A paleolimnological record of rainfall and drought from East Java, Indonesia during the last 1,400 years. *J Paleolimnol* pp 1–15. doi:10.1007/s10933-011-9564-3
- Rosqvist GC, Schuber P (2003) Millennial-scale climate changes on South Georgia, Southern Ocean. *Quat Res* 59:470–475
- Rosqvist GC, Rietti-Shati M, Shemesh A (1999) Late glacial to middle holocene climatic record of lacustrine biogenic silica oxygen isotopes from a Southern Ocean island. *Geology* 27:967–970
- Sachs JP, Myhrvold CL (2011) A shifting band of rain. *Sci Am* 304(3):60–65
- Sachs JP, Sachse D, Smittenberg RK, Zhang Z, Battisti DS, Golubic S (2009) Southward movement of the Pacific intertropical convergence zone AD 1400–1850. *Nat Geosci*. doi:101038/NGEO554
- Saji NH, Goswami BN, Vinayachandran PN, Yamagata T (1999) A dipole mode in the tropical Indian Ocean. *Nature* 401:360–363
- Schaefer JM et al (2009) High-frequency holocene glacier fluctuations in new Zealand differ from northern signature. *Science* 324:622. doi:101126/science1169312
- Schenk F, Zorita E (2012) Reconstruction of high resolution atmospheric fields for Northern Europe using analog-upscaling. *Clim Past Discuss* 8:819–868. doi:105194/cpd-8-819-2012
- Seidel DJ, Fu Q, Randel WJ, Reichler TJ (2008) Widening of the tropical belt in a changing climate. *Nat Geosci* 1:21–24
- Speirs JC, Steinhoff DF, McGowan HA, Bromwich DH, Monaghan AJ (2010) Foehn winds in the McMurdo dry Valleys, Antarctica: the origin of extreme warming events. *J Clim* 23:3577–3598
- Stager JC, Ryves D, Cumming BF, Meeker LD, Beer J (2005) Solar variability and the levels of Lake Victoria, East Africa, during the last millennium. *J Paleolimnol* 33:243–251
- Stager JC, Ruzmaikin A, Conway D, Verburg P, Mason PJ (2007) Solar variability, ENSO, and the levels of Lake Victoria, East Africa. *J Geophys Res* 112:D15106. doi:101029/2006JD008362
- Stager JC, Cocquyt C, Bonnefille R, Weyhenmeyer C, Bowerman N (2009) A late holocene paleoclimatic history of Lake Tanganyika, East Africa. *Quat Res* 72:47–56
- Stager JC, Mayewski PA, White J, Chase BM, Neumann F, Meadows ME, King C, Dixon D (2012) Precipitation variability in the winter rainfall zone of South Africa during the last 1400 years linked to the austral westerlies. *Clim Past* 8:877–887
- Stammerjohn S, Martinson D, Smith R, Yuan X, Rind D (2008) Trends in Antarctic annual sea ice retreat and advance and their relation to El Niño-Southern oscillation and southern annular mode variability. *J Geophys Res C Oceans* 113:C03S90. doi:10.1029/2007JC004269
- Steig EJ et al (2013) Recent climate and ice-sheet changes in West Antarctica compared with the past 2,000 years. *Nat Geosci* doi:10.1038/NGEO1778
- Stine S (1994) Extreme and persistent drought in California and Patagonia during mediaeval time. *Nature* 369:546–549
- Thompson D, Wallace J (2000) Annular modes in the extratropical circulation part I: month-to-month variability. *J Clim* 13:1000–1016
- Tierney JE, Oppo DW, Rosenthal Y, Russell JM, Linsley BK (2010a) Coordinated hydrological regimes in the Indo-Pacific region

- during the past two millennia. *Paleoceanography* 25:PA1102. doi:[10.1029/2009PA001871](https://doi.org/10.1029/2009PA001871)
- Tierney JE, Mayes MT, Meyer N, Johnson C, Swarzenski PW, Cohen AS, Russell JM (2010b) Late-twentieth-century warming in Lake Tanganyika unprecedented since AD 500. *Nat Geosci* 3. doi:[10.1038/NGEO865](https://doi.org/10.1038/NGEO865)
- Trenberth KE (1997) The definition of El Niño. *Bull Am Meteorol Soc* 78:2771–2777
- Trouet V, Esper J, Graham NE, Baker A, Scourse JD, Frank DC (2009) Persistent positive North Atlantic oscillation mode dominated the medieval climate anomaly. *Science* 324:78–80
- Tsonis A, Swanson K, Kravtsov S (2007) A new dynamical mechanism for major climate shifts. *Geophys Res Lett* 34:L13705. doi:[10.1029/2007GL030288](https://doi.org/10.1029/2007GL030288)
- Turner J (2004) The El Niño–Southern oscillation and Antarctica. *Int J Climatol* 24:1–31. doi:[10.1002/joc965](https://doi.org/10.1002/joc965)
- Tyson PD, Lindsay JA (1992) The climate of the last 2000 years in southern Africa. *Holocene* 2:271. doi:[10.1177/095968369200200210](https://doi.org/10.1177/095968369200200210)
- Van den Dool HM (1994) Searching for analogues, how long must we wait? *Tellus A* 46:314–324. doi:[10.1034/j.1600-0870.1994.t01-2-00006.x](https://doi.org/10.1034/j.1600-0870.1994.t01-2-00006.x)
- van Ommen TD, Morgan V (2010) Snowfall increase in coastal East Antarctica linked with southwest Western Australian drought. *Nat Geosci* 3:267–272
- Vecchi G, Soden B, Wittenberg A, Held I, Leetmaa A, Harrison M et al (2006) Weakening of tropical Pacific atmospheric circulation due to anthropogenic forcing. *Nature* 44. doi:[10.1038/nature04744](https://doi.org/10.1038/nature04744)
- Villalba R (1990) Climatic fluctuations in Northern Patagonia during the last 1000 years as inferred from tree-ring records. *Quat Res* 34:346–360
- Visbeck M, Hall A (2004) Reply. *J Clim* 17:2255–2258
- Von Gunten L, Grosjean M, Rein B, Urrutia R, Appleby P (2009) A quantitative high-resolution summer temperature reconstruction based on sedimentary pigments from Laguna Aculeo, central Chile, back to AD 850. *Holocene* 19(6):873–881
- Williams AN, Ulm S, Goodwin ID, Smith M (2010) Hunter-gather response to late Holocene climatic variability in northern and central Australia. *J Quat Sci* 25(6):831–838. doi:[10.1002/jqs.1416](https://doi.org/10.1002/jqs.1416)